The Little Ice Age climate of New Zealand reconstructed from Southern Alps cirque glaciers: a synoptic type approach

Andrew Lorrey · Nicolas Fauchereau · Craig Stanton ·
Petra Chappell · Steven Phipps · Andrew Mackintosh ·
James Renwick · Ian Goodwin · Anthony Fowler

Abstract Little Ice Age (LIA) austral summer temperature anomalies were derived from palaeoequilibrium line altitudes at 22 cirque glacier sites across the Southern Alps of New Zealand. Modern analog seasons with temperature anomalies akin to the LIA reconstructions were selected, and then applied in a sampling of high-resolution gridded New Zealand climate data and global reanalysis data to generate LIA climate composites at local, regional and hemispheric scales. The composite anomaly patterns assist in improving our understanding of atmospheric circulation contributions to the LIA climate state, allow an interrogation of synoptic type frequency changes for the LIA relative to present, and provide a hemispheric context of the past conditions in New Zealand. An LIA summer temperature anomaly of −0.56 °C (±0.29 °C) for the Southern Alps based on palaeo-equilibrium lines compares well with local tree-ring reconstructions of austral summer temperature. Reconstructed geopotential height at 1,000 hPa (z1000) suggests enhanced southwesterly flow across New Zealand occurred during the LIA to generate the terrestrial temperature anomalies. The mean atmospheric circulation pattern for summer resulted from a crucial reduction of the 'HSE'-blocking synoptic type (highs over and to the west of NZ; largely settled conditions) and increases in both the 'T'- and 'SW'-trough synoptic types (lows passing over NZ; enhanced southerly and southwesterly flow) relative to normal. Associated land-based temperature and precipitation anomalies suggest both colder- and wetter-than-normal conditions were a pervasive component of the base climate state across New Zealand during the LIA, as were colder-than-normal Tasman Sea surface temperatures. Proxy temperature and circulation evidence were used to corroborate the spatially heterogeneous Southern Hemisphere composite z1000 and sea surface temperature patterns generated in this study. A comparison of the composites to climate mode archetypes suggests LIA summer climate and atmospheric circulation over New Zealand was driven by increased frequency of weak El Niño-Modoki in the tropical Pacific and negative Southern Annular Mode activity.

A. Lorrey (✉) · N. Fauchereau · C. Stanton · P. Chappell
National Institute of Water and Atmospheric Research Ltd.,
Auckland, New Zealand
e-mail: a.lorrey@niwa.co.nz

S. Phipps
CSIRO Wealth from Oceans Flagship, ARC Centre of
Excellence for Climate System Science, Climate Change
Research Centre, University of New South Wales,
Sydney, Australia

A. Mackintosh
Victoria University Wellington, Antarctic Research Centre,
Wellington, New Zealand

J. Renwick
Victoria University Wellington, School of Geography,
Earth Sciences, Wellington, New Zealand

I. Goodwin
Marine Climate Risk Group,
Climate Futures and Department of Environment
and Geography, Macquarie University,
Sydney, Australia

A. Fowler
University of Auckland, School of Environment,
Auckland, New Zealand

1 Introduction

1.1 Background

The Little Ice Age (LIA) is widely associated with terminal positions of mountain glaciers beyond their modern extent (Mann 2002). Instrumental climate evidence and documentary archives (both literary and illustrative) from many Northern Hemisphere sites have linked LIA glacier activity to past climate conditions different from today (Bradley et al. 2003). For New Zealand, instrumental observations and written historic accounts of weather and climate did not exist with regularity until the early-to-mid 1800s. Early Southern Alps observations in the mid-to-late 1800s indicate many glaciers had ice margins that were advanced close to freshly deposited late Holocene moraines when the LIA was ending in the Northern Hemisphere (Von Haast 1879; Ackland 1892; Sealy 1892). Complementary proxy evidence of past temperature (Cook et al. 2002) and palaeohydrology changes (Lorrey et al. 2008) suggest the LIA signal, including prominent multi-decadal climate variability, was registered locally in New Zealand. That evidence suggests a local 'LIA' event may have begun in the mid 1400s that was subtly different from the Northern Hemisphere counterpart. The Southern Alps moraine chronology includes features that correspond to the ~1450–1850 CE interval. They are dated using historical accounts, and extended back in time with lichenometry, radiocarbon dating, and surface exposure age techniques (see Lorrey et al. 2008; Putnam et al. 2012 for relevant references).

Modern studies of Southern Alps glaciers (see Fig. 1 for location) indicate an acute sensitivity to regional climate conditions that are controlled by atmospheric circulation patterns (see Chinn et al. 2012 for an overview of relevant literature). The relative importance of atmospheric temperature and precipitation on controlling glacier mass balance has been debated. However for Southern Alps glaciers, which exist in a temperate-humid environment, the main factor that determines net loss or gain of ice is the near-surface air temperature, especially during the summer months (Anderson and Mackintosh 2006; Purdie et al. 2011). Annual monitoring of snow and ice coverage for the Southern Alps since the late 1970 s has improved the understanding of New Zealand glacier responses to climate variability. Chinn et al. (2012) developed a 42-year proxy record of glacier mass balance and the equilibrium line altitude (ELA) for a key

set of index glaciers based on an end of summer snow-line (EOSS) survey. The EOSS survey consists of oblique aerial photographs taken in March each year, and they indicate Southern Alps glaciers are highly sensitive to inter-annual climatic variability. ELA position changes are currently proposed to be highly correlated with summer climate conditions, and most notably air temperature anomalies. This suggests the general character of the ablation season (and thus temperature), and changes from year-to-year, significantly contributes to glacier mass balance fluctuations.
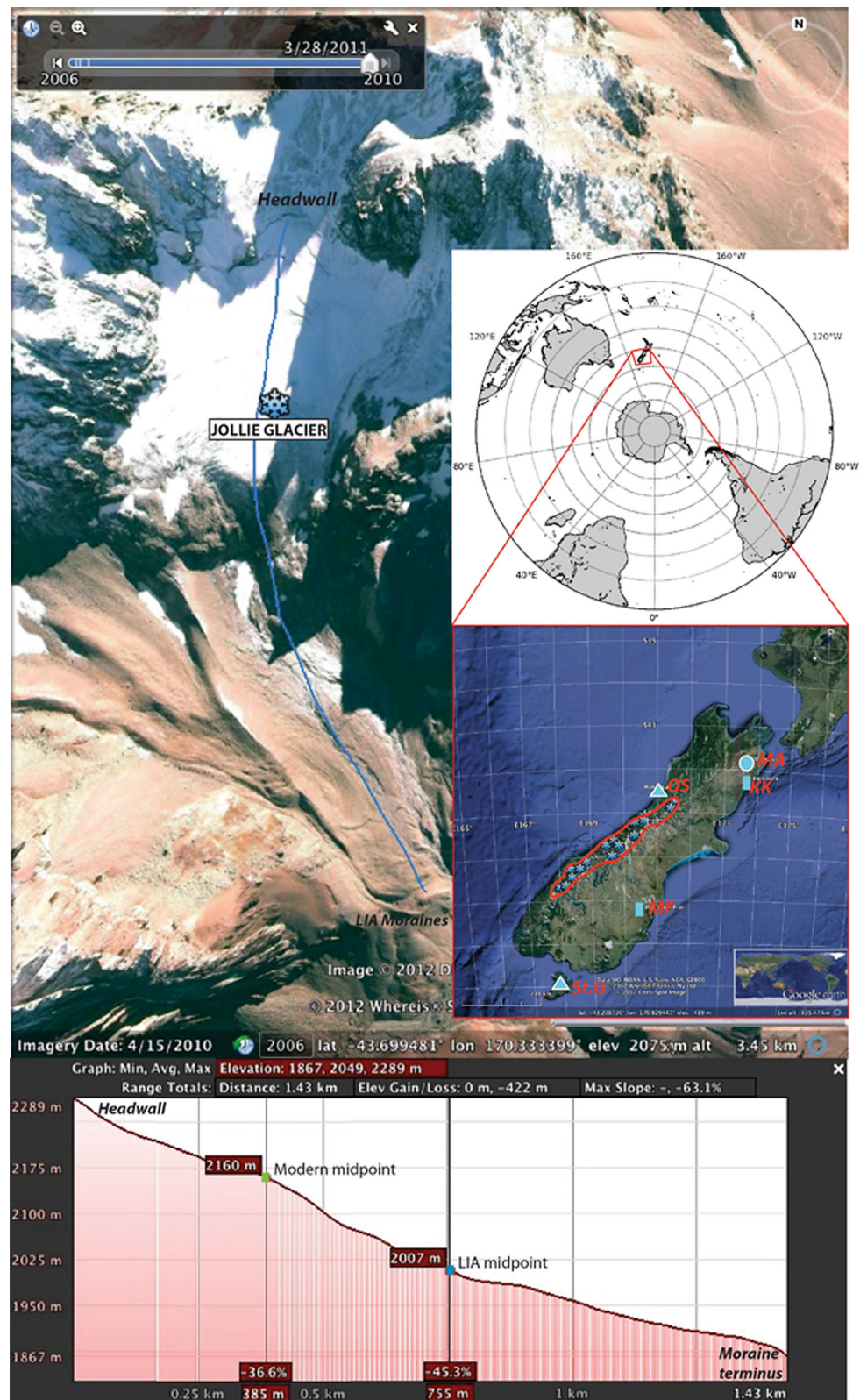
Chinn (1996) previously noted that the mid-point of New Zealand cirque glaciers (a Southern Alps glacier sub-type) is situated close to the ELA, and mean elevation changes (which can be tracked using total glacier length) could be used as a modern equilibrium line altitude (ELAm) proxy. ELAm altitudinal position reflects seasonal mass balance activity. Therefore, for fast-response cirque glaciers, the altitude difference between a modern ELA (ELAm) and a palaeoELA (ELAp) can also be related to temperature change using the environmental lapse rate ($-0.0065\,°C$ per meter increase in elevation, though in New Zealand this rate may be lower). The concept espoused by Chinn (1996) is essentially an application of a toe-to-headwall altitude ratio (THAR), which is useful for calculating changes in ELA for glaciers with simple geometries (Meierding 1982). Past temperature changes have been recently derived using ELAs of pre-industrial Holocene moraines in front of the Cameron glacier (Putnam et al. 2012), part of the set of Southern Alps cirque glaciers that were assessed by Chinn (1996).

1.2 Purpose

At present, there is abundant existing information that can be 'mined' to learn more about mean climate state changes for several critical intervals during the Holocene, including the LIA. This is an area that is currently underexploited in palaeoclimatology in the Southern Hemisphere, which has been acknowledged by the PAGES 2k initiative. As such, new assessments of existing Southern Hemisphere proxy data, including those from New Zealand, are an important and integral part of advancing the present understanding of global palaeoclimate change.

LIA mean austral summer temperature anomalies for selected cirque glacier sites spread across the Southern Alps of New Zealand are reconstructed in this study based on palaeoequilibrium line altitudes, expressed by differences between modern and LIA glacier mid-points (proxies for ELAm and ELAp). These ELA-based temperature anomalies were subsequently used to identify a set of modern analog seasons from local and global data

Fig. 1 Example of a GoogleEarth™ photograph of a Southern Alps cirque glacier (Jollie glacier). The long axis of the modern glacier and the palaeoglacier correspond to the *blue line* connecting the cirque headwall to the Little Ice Age moraine complex. The location of New Zealand within the Southern Hemisphere is seen in the *black* and *white inset map* (to the *right* of Jollie glacier). The South Island of New Zealand is seen below the *inset map*, and the *red line* circumscribes the Southern Alps. The *small blue symbols* inside that boundary indicate the distribution of cirque glaciers studied by Chinn (1996) that were assessed in this study. Local palaeoclimate proxy sites outside the Southern Alps are noted by *triangles* (tree rings); *rectangles* (borehole) and *circle* (moraines). OS = Oroko Swamp, MA = Mount Alarm, KK = Kaikoura, MF = MacRae's Flat, St.Is = Stewart Island. A GoogleEarth™ elevation profile tool screen shot (*lower part* of the figure) illustrates the cross-section from the cirque headwall to the Little Ice Age (LIA) moraine complex. The modern glacier midpoint is noted with a *green box* on that profile while the LIA midpoint is noted by a *blue box*. The elevations from this profile are recorded in Table 1 and were used to calculate ELAm and ELAp

(NIWA's Virtual Climate Station Network, NCEP/NCAR Reanalysis 1 and HADSST3) that were composited to reconstruct mean summer climate conditions assumed to be representative of what may have occurred during the LIA. Three key questions are posed from the results of these reconstructions:

- What atmospheric circulation pattern contributed to New Zealand glacial advances during the LIA?
- What were the associated climate changes for New Zealand that were induced by atmospheric circulation during the LIA?
- What was the regional and hemispheric context for the ocean and the atmosphere that contributed to New Zealand's LIA climate signatures?

A test of the approach employed was to compare the results for inferred anomalies at the both regional and hemispheric scales to existing proxy data of past LIA climate conditions. We discuss of some of the key reconstructed elements (regional and Southern Hemisphere atmospheric circulation, New Zealand land temperature & precipitation anomalies, and regional/global sea surface temperature anomalies) with regard to previously published work, and suggest the possible role hemispheric-scale climate drivers played in dictating regional atmospheric circulation patterns across New Zealand during the LIA.

2 Details about synoptic types, teleconnections and palaeo-circulation reconstructions

New Zealand is an ideal setting to employ circulation-based palaeoclimatology techniques because of a hypersensitivity to changes in mid-latitude westerly circulation. The variability of synoptic type occurrences can disrupt, diminish, or enhance prevailing westerly atmospheric circulation that flows across New Zealand (Jiang et al. 2012). Prominent NE-SW trending axial mountain ranges (>3,000 m on the South Island) cause orographic precipitation patterns that are typified by disparate west-east hydrologic contrasts. The precipitation anomalies that are linked to synoptic type frequency changes are often considered to be more spatially distinct than temperature anomalies for New Zealand (Kidson 2000). However, prominent temperature contrasts also occur for western, eastern, northern and southern NZ climate districts due to anomalous flow that is generated by synoptic-scale pressure anomalies (Renwick 2011). Incident airflow across the surrounding ocean waters uptakes and transmits the temperature characteristics of oceanic currents and fronts positioned close by (ranging from warm subtropical to cool subantarctic) onto the land.

Multiple regional climate drivers combine to dictate oceanic temperature anomalies that influence New Zealand from year-to-year (including exogenic and anthropogenic forcings). However, it is inevitably atmospheric circulation that creates a link between the oceanic domain and terrestrial climates across the country (Folland and Salinger

1995). The largely 'maritime' climate with negligible continental feedbacks means terrestrial temperature anomalies that occur in the absence of radiative forcing (from greenhouse gases or insolation) arise from the incident direction of atmospheric flow. Hence, synoptic type frequency changes can produce significant terrestrial temperature anomalies for New Zealand because they dictate how the temperature characteristics of oceans that surround the country are conveyed to the land.

Kidson (2000) defined 12 atmospheric circulation synoptic types for the New Zealand domain, subsequently aggregated into 3 regimes (Trough, Zonal, Blocking; See Fig. 2). The method used to define the synoptic types is based on a k-means clustering of a twice-daily geopotential height field at 1000 hPa in EOF space (space spanned by the first 5 EOFS). New Zealand synoptic types have both seasonal and regional climate driver associations (with the Southern Annular Mode (SAM), El Niño-Southern Oscillation (ENSO) and the Inter-decadal Pacific Oscillation (IPO) being three important phenomena to note (see Kidson 2000; Jiang et al. 2012; Lorrey et al. 2012 for details). Jiang et al. (2012) recently espoused how these drivers combine in different ways to generate synoptic type frequency changes, which in turn leads to regional climate anomalies that are induced by orographic effects.

For example, ENSO changes the energy distribution in the tropical and extratropical atmosphere, which can effectively "load the dice" (i.e., either increases or decreases) for the probabilistic occurrence of daily synoptic weather types at a regional scale. Once the effects of the daily weather types are integrated at longer time-scales (e.g., seasonal, annual, decadal, etc.), changes in weather regime frequency can manifest as a significant shift in the base climate state. Application of this concept has recently been assessed with regard to New Zealand palaeoclimate reconstruction by Lorrey et al. (2007, 2008, 2012).

It is important to note that different climate driver combinations can generate similar synoptic type sets. This means attributing a lone climate driver as a root cause of a regional climate anomaly remains difficult. The only assumption that can be made is the response of any given site to a synoptic type change (via a change in incident circulation direction) remains consistent through time. This local response is assumed to remain stable, despite teleconnection instabilities for the very climate drivers that mutually generate the synoptic types (Jiang et al. 2012). By focusing on synoptic type frequency changes, an emphasis can be placed on the invariant part of the relationship between local climate anomalies and regional-scale circulation, which helps to circumvent issues of remote climate driver teleconnection instabilities through time when reconstructing past climate.
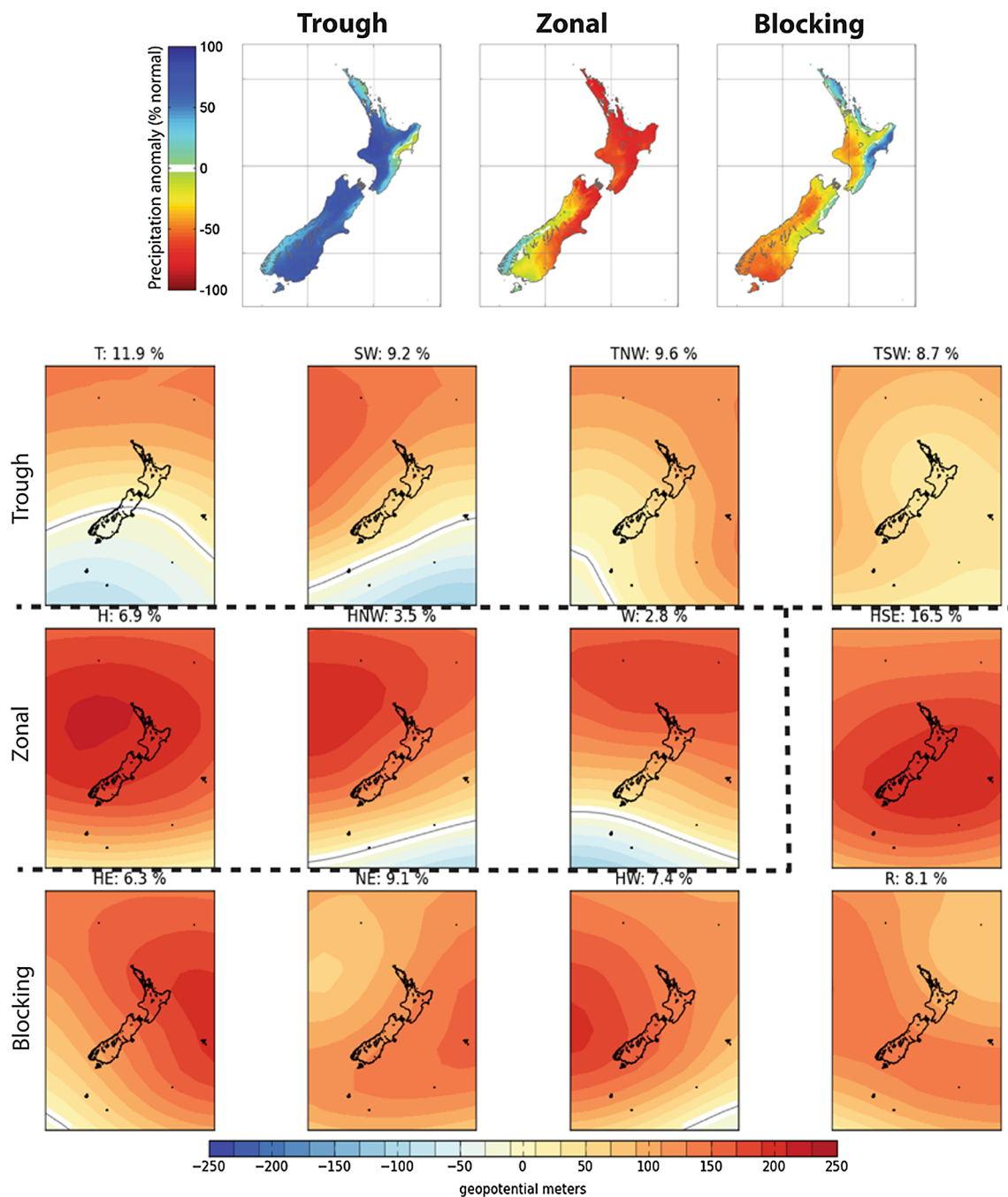
Fig. 2 Precipitation anomalies for New Zealand's climate districts (*top*), based on the analysis of Renwick (2011) that correspond to Trough, Zonal and Blocking climate regimes (after the classification of Kidson 2000). Synoptic types (*bottom*) contained in each of the Kidson regimes that are observed on weather time scales (% occurrence for DJF shown above each type). *Shaded contours* represent anomalies (m) at the 1,000 hPa geopotential height (*red shades* = positive; *blue shades* = negative). Figure is modified from Lorrey et al. (2012)

3 Data and methods

3.1 Equilibrium line altitude (ELA) reconstruction of temperature

Chinn (1996) outlined ELAm and reconstructed ELAp for the LIA based on palaeoglacier length as indicted by

geomorphic constraints using a set of 26 cirque glaciers. In most cases Chinn (1996) used recessional moraine sequences fronting each glacier, but lateral moraines and scoured bedrock surfaces can also be used (Table 1). The difference between ELAm and ELAp provided by Chinn (1996) multiplied by the environmental lapse rate was used to arrive at a palaeotemperature for the LIA at each glacier

Table 1 Details of cirque glaciers assessed in this study, including ELAm and ELAp derived from maps (Chinn 1996) and Google Earth™

Glacier name	Latitude	Longitude	Chinn (1996) ELAm	Chinn (1996) ELAp	Aspect (azimuth)	Elevation change (m)	ΔT (degrees C)	ΔT (degrees C)	Google earth ELAm	Google earth ELAp	Elevation change (m)	ΔT (degrees C)
Greenlaw	−43.006108°	171.419497°	1,740	1,585	81	78	−0.51	−0.51	1,800	1,760	40	−0.26
Crow	−43.346222°	170.998122°	1,675	1,494	165	91	−0.59	−0.59	1,861	1,766	95	−0.62
Cameron	−42.934067°	171.505139°	1,830	1,646	230	92	−0.60	−0.60				**0.81**
Avoca	−43.043031°	171.405812°	1,860	1,798	130	31	−0.20	−0.20	1,979	1,898	81	−0.53
Temple	−44.146466°	169.709872°	1,800	1,768	156	16	−0.10	−0.10	1,961	1,839	122	−0.79
Hopkins	−43.942569°	169.887499°	1,860	1,798	239	31	−0.20	−0.20	2,053	1,993	60	−0.39
Turnbull	−43.877607°	169.850303°	1,920	1,920	92	0	0.00	0.00	1,779	1,717	62	−0.40
Jollie	−43.697778°	170.330000°	2,080	1,829	195	126	−0.82	−0.82	2,160	2,007	153	−0.99
Cass	−43.652675°	170.315493°	2,190	1,951	174	120	−0.78	−0.78	2,226	2,201	25	−0.16
Caples	−44.801851°	168.182845°	1,340	1,265	191	38	−0.25	−0.25	1,533	1,479	54	-0.35
Fraser	−44.786354°	168.186884°	1,555	1,463	194	46	−0.30	−0.30	1,650	1,618	32	−0.21
Frances	−44.596521°	168.395713°	1,800	1,615	170	92	−0.60	−0.60	2,086	2,023	63	−0.41
Hunter	−44.094444°	169.646667°	1,830	1,768	275	31	−0.20	−0.20	1,903	1,767	136	−0.88
Hunter2	−44.120833°	169.636111°	1,875	1,829	290	23	−0.15	−0.15	1,922	1,900	22	−0.14
Mistake	−44.843612°	168.015261°	1,000	823	150	89	−0.58	−0.58	1,209	1,034	175	−1.14
Silver	−44.416907°	168.348990°	1,555	1,128	289	214	−1.39		2,073	1,543	530	_−3.45_
Pyke	−44.803611°	168.178333°	1,630	1,615	259	7	−0.05	−0.05	1,621	1,605	16	−0.10
Falls Creek	−44.824221°	168.015937°	1,175	1,082	128	46	−0.30	−0.30	1,209	1,100	109	−0.71
Arawhata	−44.403039°	168.646438°	1,220	1,097	282	61	−0.40					
Pear Drop	−44.251904°	168.849048°	1,705	1,554	253	75	−0.49	−0.49	1,903	1,797	106	−0.69
Clarke	−43.873611°	169.451667°	1,525	1,097	126	214	−1.39	−1.39	1,168	1,148	20	−0.13
Browning Creek	−43.850548°	169.836463°	1,980	1,646	282	167	−1.09	−1.09	1,868	1,773	95	−0.62
Mahitahi	−43.777546°	169.699115°	1,295	1,158	297	68	−0.44		1,984	1,480	504	_−3.28_
Perverse Creek	−43.319570°	170.612898°	1,540	1,402	270	69	−0.45					
Gunn	−43.368294°	170.327343°	1,660	1,173	133	243	−1.58	−1.58	1,438	1,348	90	−0.59
Taramakau	−42.899444°	171.486667°	1,795	1,585	106	105	−0.68	−0.68	1,657	1,551	106	−0.69
							26 glaciers	22 glaciers				22 glaciers
						Mean	−0.54	−0.52			Mean	−0.52
						Median	−0.47	−0.50			Median	−0.56
						Stdev	0.42	−0.42			Stdev	0.29

Reconstruction for Cameron glacier used in this study is taken from Putnam et al. (2012)

site. Topographic maps resolved at 1:50,000 scale and 20 m contours were employed in that study to determine the elevation estimates for ELAm and ELAp (i.e., use of a geodetic method).

Digital elevation models combined with satellite photography in Google Earth[TM] (GE) now allow a reassessment of ELAm and ELAp for Southern Alps cirque glaciers relative to the map-based approach used in Chinn (1996). GE was used to reassess the midpoints (halfway between highest and lowest elevation of vertically contiguous ice) for modern and LIA-reconstructed cirque glaciers (see Table 1). Sources and precision of GE geospatial data and limitations are discussed in more detail in the Supplementary material.

We consider cirque glacier DEM-based elevation profiles created in GE as an improvement over previous work, which combined vertical aerial photos and traditional topographic maps with contours spaced 20 m apart (i.e., a geodetic method). This statement is based on a few salient points: multiple operators can examine each glacier site and repeat the analyses, and biases that could potentially be introduced by manual interpolation between topographic map contours can be avoided. While the overall elevation model in GE may also be different between GE and topographic map projections, it is the relative elevation changes for ELAm and ELAp that matter for the exercise of palaeotemperature reconstruction. This point is demonstrated by comparing both temperature reconstructions and circulation reconstructions that employ the Chinn (1996) approach and also the GE approach for determining ELAm and ELAp.

Reconstructed LIA cirque glacier lengths using GE were based on the lowest elevation the glacier would have reached during the LIA as determined by geomorphology. In most cases, an end moraine was used (similar to the approach of Putnam et al. 2012) to mark the terminal position of each glacier in GE. However in a few cases, scouring of bedrock on steep slopes and relative degree of weathering distal to the current glacier terminus were employed when an LIA moraine was not obvious. We recognize that the LIA moraine sequences for many glaciers across the Southern Alps have still not been directly dated. However, for many Southern Alps glaciers, including some assessed in this study (Greenlaw, Crow, Cameron, Frances and Turnbull), early photographs, survey maps or historic accounts of ice positioned proximal to moraines reveal a LIA position (Gellatly 1982; T. Chinn, personal communication). The geomorphic expression of the LIA morphosequence is also well-recognized (see examples in Chinn 1996; Winkler 2000; Mckinzey et al. 2004; Schaefer et al. 2009), often consisting of sets of tightly spaced moraines with sharp crests that are absent of major vegetation. LIA moraines appear stark in contrast to older moraine sequences deposited during the Holocene that are positioned adjacent to or distal to the LIA sequences.

Because the LIA moraine suites are often compressed within a short distance of one another, a palaeotemperature assessment for the composite LIA morphosequence (and therefore average, temporally-integrated conditions that correspond to the depositional time scale for LIA) can be derived. In some cases, geomorphic clues as to the relative age of a moraine were not evident, or the glacier was obscured in GE imagery, and this meant some of the glaciers were rejected for that analysis (Perverse Creek and Arawhata). In all cases, a transect running along the central axis of each glacier that was 'clamped to the ground' from the highest point of observed ice, through the lowest point of modern ice to the LIA margin were generated in GE. These transects were used to determine the midpoints (distance in km on the ground) for modern and LIA cirque glaciers. The elevation for both the modern and LIA glacier midpoints were taken from the LIA profiles and are reported in Table 1. We discuss the possible ramifications of not incorporating former ice thickness in the ELAp calculation and caveats in the Supplementary material.

It is also recognized that accumulation changes from wind-blown snow drifting could have an influence on some glaciers; however, this would be dependent on surrounding topography, elevation, shading, aspect of the catchment and availability of local snowpacks for winnowing and redeposition of snow. Therefore, this influence would be glacier-dependent. The sample set of 22 glaciers helps to minimize the effects that any individual glacier would have had on the reconstruction from this type of influence.

3.2 Identification of LIA modern analogs

The New Zealand Virtual Climate Station Network (VCSN; Tait et al. 2006) includes 13 daily climate variables interpolated on a regular (~ 5 km) grid covering the whole of New Zealand using a thin-plate smoothing spline model. This model incorporates two location variables (latitude and longitude) and a third "pattern" variable. For temperature, elevation is included in the model, while for rainfall the 1951–1980 mean annual rainfall digitized from an expert-guided contour map (Tait et al. 2006, 2012) is employed.

The closest VCSN grid point (or "agent") to each cirque glacier was identified, and the austral summer (December–February; DJF) temperature anomalies for 1972–2010 were calculated from the corresponding time-series of daily temperatures. No VCSN agent was used more than once, so there are no repeat time-series used for the set of cirque glacier temperature anomaly reconstructions. Linear trends were subtracted from the seasonal anomaly time-series (see

below, Sect. 3.4) and the results partitioned into quintiles (defined by the 20, 40, 60 and 80th percentiles).

The glacier-based temperature anomalies reconstructed using ELAm and ELAp (see Table 1) were then compared to the temperature anomaly ranges for each quintile. Two glaciers had a reconstructed temperature anomaly that was not in the modern DJF range (Silver and Mahitahi; geomorphic interpretations were difficult for these sites) so they were rejected for further analyses. This meant that only 22 of the 26 glaciers from Chinn (1996) are used in this study. The years within each quintile that encompassed the reconstructed LIA temperature anomaly were then selected as modern analogs for further analysis.

3.3 Anomalies in synoptic type frequency and statistical significance

For each site and the selection of analog years, anomalies in each synoptic type's (k) frequency were calculated as the deviation of the frequency of the corresponding type from its' climatological frequency. Changes were expressed in terms of a percentage, so that -100 % indicates that the type k is never observed during the analog years, and $+100$ % indicates a two-fold increase. To test the significance of synoptic type frequency changes, a Monte-Carlo approach essentially following the one exposed in (Cassou 2008) and Riddle et al. (2013) was employed. This Monte-Carlo approach is based on artificial realizations of the time-sequence of the 12 Kidson types that are generated using a 12 states discrete Markov chain constrained entirely by: (1) the observed probability of occurrence of each type (calculated over the DJF 1972/73–2009/10 period) and (2) a matrix describing the probability of transitions from day $n - 1$ to day n from type i to type j.

10,000 simulations were performed independently for each of the 38 DJF seasons, leading to 380,000 seasons whose properties (types distribution and transitions) are identical to the observed sequence of Kidson types. The change in probability of observing the type k for the analog seasons is then calculated for each of the 10,000 synthetic realizations. The 90th and 95 % confidence limit is drawn from this null distribution, so that the observed anomaly in the frequency of type k is considered significant at the 95 % confidence level if it is below the corresponding 5th percentile for negative anomalies (above the 95th percentile for positive anomalies).

3.4 Composite analyses

In addition to synoptic type frequency changes, geopotential height at 1,000 hPa (z1000) and sea surface temperature (SST) composite anomalies were generated for the ensemble (i.e., across the 22 sites) using the National Center for Environmental Research/National Center for Atmospheric Research (NCEP/NCAR) Reanalysis version 1 (Kistler et al. 2001) and HadSST (Rayner et al. 2003) datasets respectively. Geographical domains for these composites encompassed New Zealand, the Southwest Pacific and the whole Southern Hemisphere. For both z1000 and SSTs, a seasonal map was generated for each site by subtracting the long-term climatic mean (climatology) from each analog. All the seasonal analogs (converted to anomalies) were averaged to produce a mean circulation pattern that could have generated past temperature anomalies at each glacier site as indicated by the ELA-based reconstruction. An example of this procedure using z1000 at the regional scale is shown for Jollie glacier in Fig. 3. The synoptic grid circumscribing New Zealand is contained within the larger hemispheric structure. All three spatial scales (New Zealand, South Pacific, and Southern Hemisphere) are drawn from the same reanalysis data sets. The "synoptic grid" presented is the domain (160°E–175°E, 25°S–55°S) used by Kidson (2000) to identify regional weather regimes.
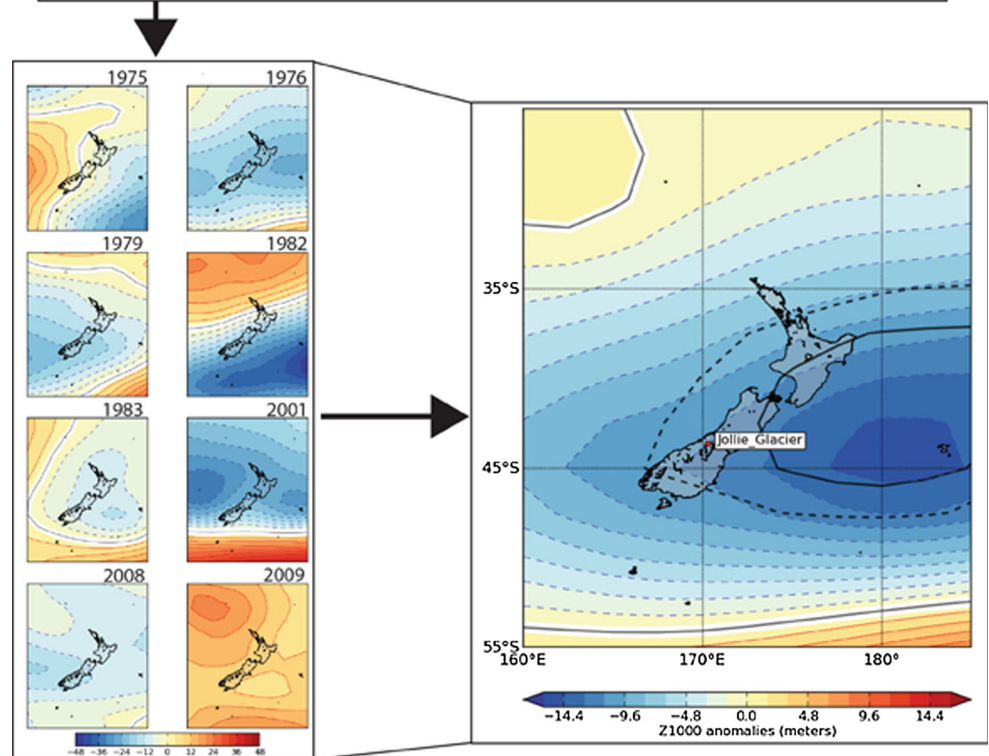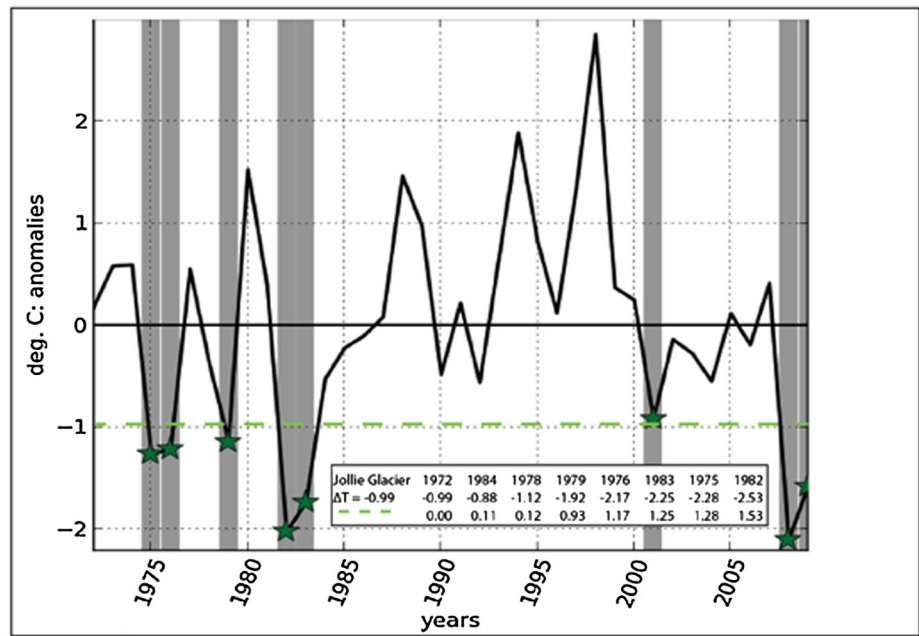
Subsequently, ensemble composites, based on the combination of mean circulation patterns for all 22 sites, were generated. When the ensemble composite was made, some seasons were selected as analogs by more than one glacier site. The repeat analog seasons provided weighting to specific circulation patterns that were more common within the analog set (160 analogs in total chosen from 38 seasons). For full field anomalies (z1000 and SST) significance was assessed using a simple two-tailed Student t test. We knowingly made the choice to use analog season repeats as a weighting mechanism for the ensemble composite, despite a resulting artificial inflation of t-test significance. The reason for this choice is that the use of weighting indicates the most common anomalies between reconstructions that were independently determined at each glacier site. Separate analyses with and without use of weighting for specific analog seasons produced similar results for the spatial anomalies across the SH (see Supplement). National-scale climate anomaly maps for precipitation and temperature were composited using VCSN data and the same analog seasons (and weighting) identified by the quintile-based selection approach. The ensemble mean z1000 pattern, which covers all of New Zealand, was also expanded spatially for the discussion to show regional (southwest Pacific) and hemispheric circulation patterns.

4 Results

4.1 Austral summer temperature reconstructions based on Southern Alps cirque glacier ELA changes

The inter-comparison of LIA temperature reconstructions using map-based and GE-based methods for 22 Southern
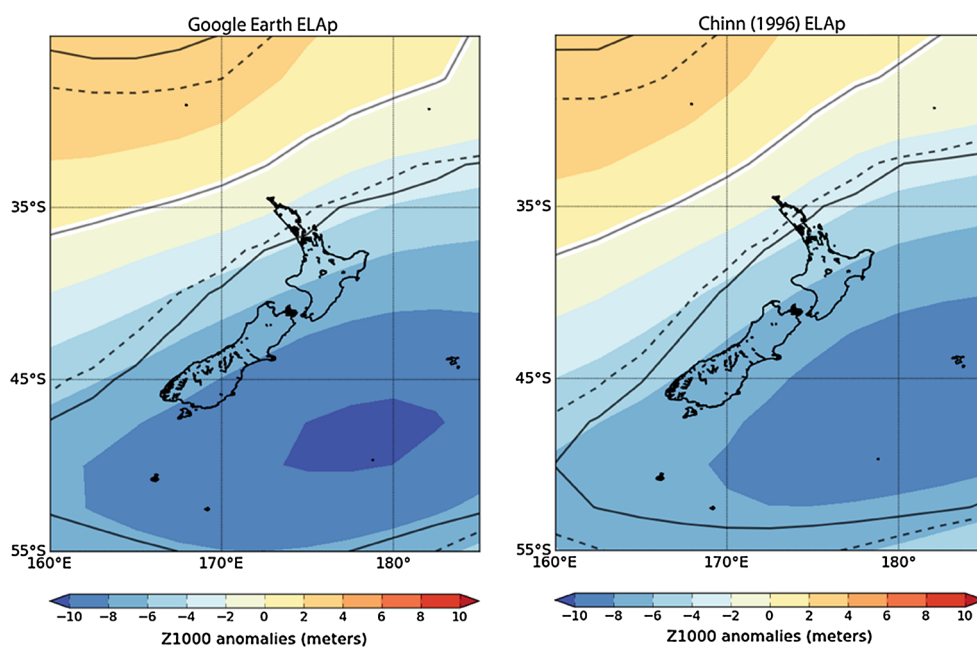
Fig. 3 (Top) Detrended DJF temperature series for the VCSN grid corresponding to the Jollie Glacier. *The green dashed horizontal line* indicated dT (−0.99 °C) reconstructed for the LIA at Jollie Glacier. This temperature anomaly falls into quintile 1, and the *green stars* highlight the analog seasons in that quintile. The individual analog seasons in quintile 1 are also listed in the *lower right part* of the temperature anomaly time series. The temperature anomaly and absolute difference in temperature between the seasonal anomaly and the reconstructed temperature for Jollie Glacier are listed below each analog season, respectively. (*Lower left*) z1000 plots (contour in meters) are shown for each of the analog seasons which were combined to generate an ensemble composite anomaly pattern (*right*). The 90th and 95th percent (*dashed* and *solid black lines*) confidence intervals are superposed on the plot

Alps cirque glaciers are shown in Table 1. From the 22 glaciers used in both studies, the ELA-derived average austral summer temperature depression is −0.52 °C, with a median of −0.56 °C (±0.29 °C). The spread of the reconstructed temperatures for the cirque glacier sites indicate summer temperature anomalies between −0.27 and −0.85 °C relative to present, which can probably be expected for the wide-array of sites (with varying aspects, slopes, shading and elevation) that were employed. Use of the Chinn (1996) ELA values results in a LIA summer temperature anomaly of −0.52 °C, with a median of −0.50 °C (±0.42 °C). The common result suggests the GE approach for calculating past temperatures is robust when compared to other geodetic methods where ELAm and ELAp are derived, albeit with subtle differences for individual reconstructions across all the sites.

Fig. 4 GoogleEarth[TM] (GE) based (*left*) and geodetic-based (*right*) reconstruction (using ELA changes identified by Chinn 1996) for austral summer (December–February) 1,000 hPa geopotential height (z1000) derived from the VCSN/analog circulation pattern selection method. The ensemble composite anomaly patterns for each reconstruction were based on the same 22 glaciers. Geopotential height anomaly contours are in meters. The 90th and 95th percent (*dashed* and *solid black lines*) confidence intervals are superposed on the plot

4.2 Ensemble composite summer z1000 anomaly for the LIA

The ensemble composite z1000 patterns for both the geodetic (Chinn 1996) and GE-based methods are similar for New Zealand (Fig. 4). Both patterns show a 'low' that extends from the south Tasman Sea across the South Island to the northeast of the Chatham Islands. This pattern is characteristic of a 'trough' regime, which would have generated westerly and southwesterly flow across much of the country. The highest confidence in both reconstructions is over the South Island, the south Tasman Sea and to the southeast of the country. The z1000 plot based on Chinn (1996) and that derived using GE measurements have similar characteristics across the SW Pacific and the Southern Hemisphere (not shown). The map-based and the GE-results are considered equivocal; we move forward in this study utilizing the results from the GE-based LIA temperature reconstructions.

4.3 Synoptic type changes

The synoptic type frequency changes that produced the mean LIA circulation pattern (Fig. 5a) appear small relative to the long-term DJF climatic mean (1972–2010). However, as stated above (section) even small variations in synoptic weather types can produce quite stark regional climate anomalies via orographic effects (Renwick 2011). The 22-glacier ensemble composite indicates an increase in 'trough' regime synoptic types (except the 'TSW' type), and reductions in 'blocking' types during the LIA (Fig. 5b). 20 of 22 glaciers showed an increase for at least two out of four trough synoptic types (19 of 22 glaciers indicated an increase in the 'SW' and/or the 'T' type), while the same number of

glaciers showed a prominent decrease in the 'HSE' blocking type category. The overall pattern for zonal synoptic type changes was weakly positive (and significant at the 90 % confidence level for 12 glaciers).
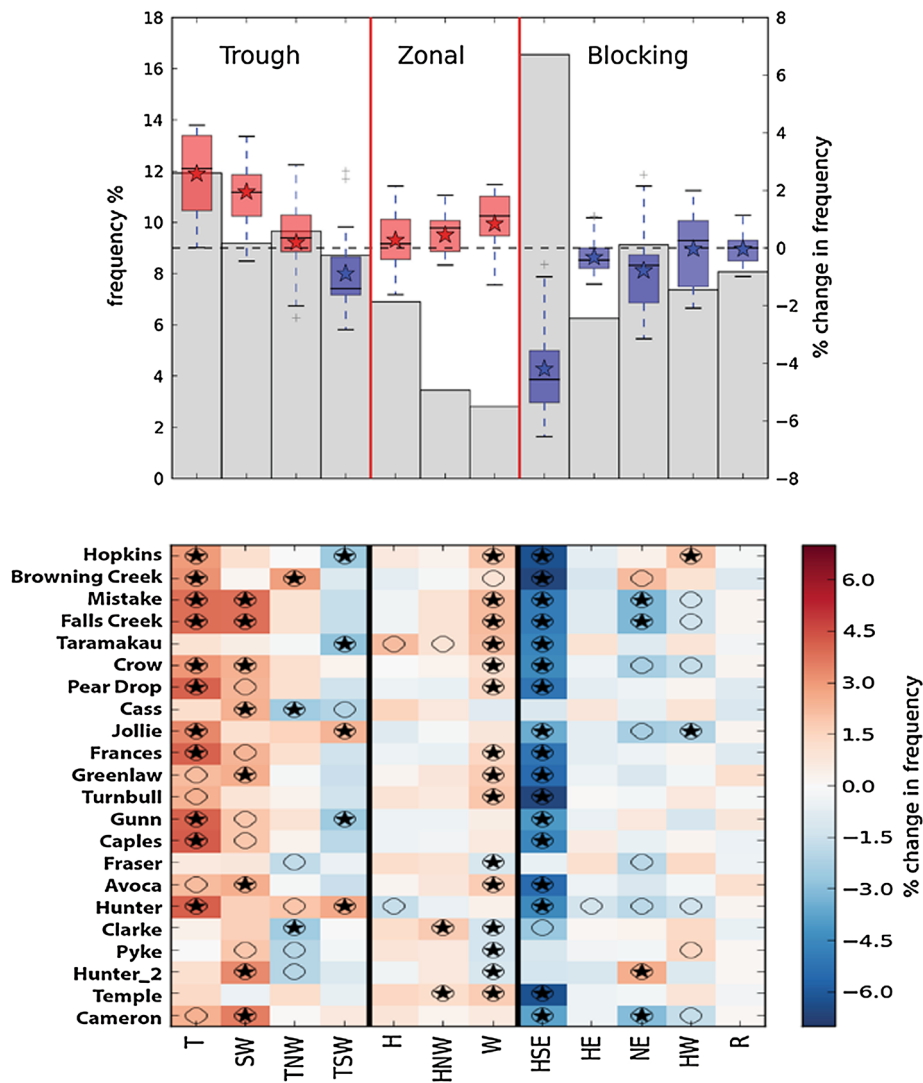
The Monte-Carlo based test indicates 16 of the 22 cirque glaciers show a significant increase (p value ≤0.05) in one or more of the trough synoptic types. 14 of those 16 glaciers also indicate a significant decrease in the 'HSE' blocking type. Significant synoptic type changes were also noted for cirque glaciers across a wide variety of aspects and also relative to latitude. The largest and most significant (and common) change for the set of glaciers was a reduction in the frequency of the 'HSE' Blocking type (significantly negative for 17 of 22 glaciers at the 95 % confidence level).

4.4 National-scale climate patterns reconstructed for New Zealand during the LIA

The VCSN-based climate anomalies for New Zealand during the LIA were produced from the analog years used to generate the circulation pattern seen in Fig. 4a. Reconstructed temperature and precipitation anomalies are spatially heterogeneous for the LIA across New Zealand (Fig. 6). Negative temperature anomalies are observed across much of the country, with a gradient characterized by stronger negative anomalies in western and southern regions relative to northern and eastern areas (Fig. 6a). The areas with the least negative anomalies for both the North and South Island are on the leeward side of mountain ranges (relative to westerly and southwesterly flow).

The spatial anomalies seen for LIA precipitation (Fig. 6b) indicate a major increase for most of the Southern

Fig. 5 (*Top*) Climatological frequency of synoptic types (*grey bars*) nested in three basic climate regimes (trough, zonal, blocking; after Kidson 2000) for New Zealand during summer based on 1972–2010 VCSN data. Synoptic type frequency changes that were implicated by all of the cirque glacier temperature reconstructions for the LIA are superposed on the climatology. The median and mean (*horizontal black line* = median; *star* = mean) and spread are shown by the *superposed box* and *whisker plot* (*red* = increase, *purple* = decrease). (*Bottom*) Frequency changes for each synoptic type as indicated by the ELA-based reconstruction of summer temperature during the LIA for 22 Southern Alps cirque glacier sites. 90th and 95th percent confidence interval for synoptic type changes at individual sites are indicated by the *open circle* and *star*, respectively

Alps, however the anomalies for the eastern South Island and central/north Otago are negligible. The LIA precipitation pattern for the North Island indicates close to normal or slightly above normal precipitation during summer, with the strongest positive anomalies centered on the Tararua Ranges north of Wellington, the central volcanic plateau and near Mt. Taranaki. When compared to Kidson (2000) and Renwick (2011) archetypal patterns, both temperature and precipitation are most similar to 'trough' regimes described in both of those studies.

5 Discussion

5.1 Comparison to proxy evidence across the Southern Hemisphere

Proxies that covered all or a significant part (at least ∼100 years) of the LIA (defined as ∼1450–1850 AD

here) were drawn from a Southern Hemisphere high-resolution proxy review (Neukom and Gergis 2011). We compare the results of our reconstruction (see Fig. 7) to local, regional and hemispheric temperature conditions inferred by SH proxy data. It is recognized that (1) many proxy archives contain prominent climate variability within the LIA; as such the mean state was calculated for these proxies where possible, and (2) there may be key similarities (differences) to note where the confidence in the z1000 and SSTa reconstructions are high (low). A summary of some key proxies in the regional descriptions in the following section can be found in Table 2.

5.1.1 New Zealand

In New Zealand, many tree ring records (some of which have an associated temperature reconstruction) cover part or all of the LIA. We make use of the reconstructions that are only derived from single sites because it can be safely
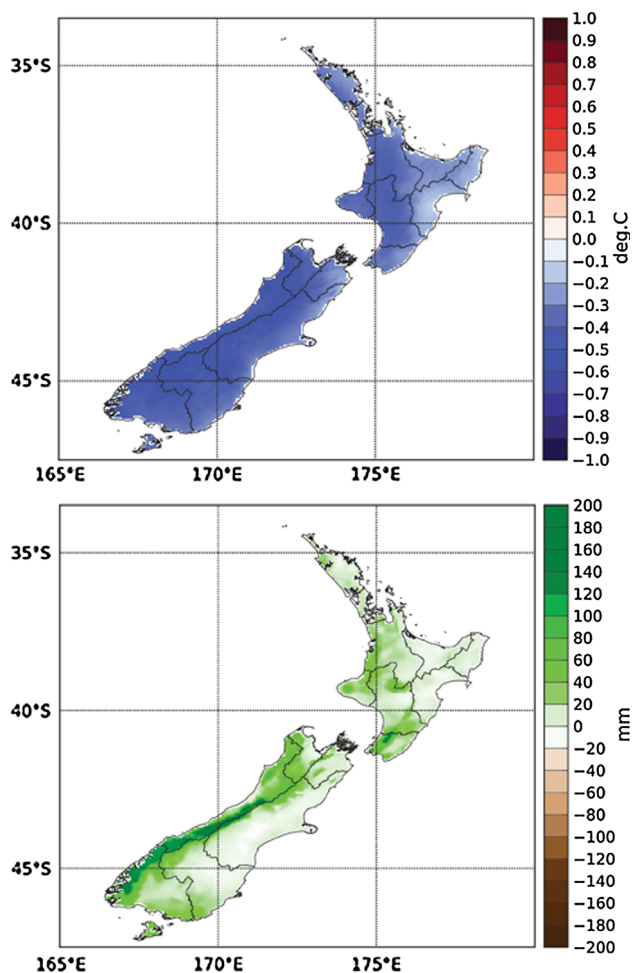
Fig. 6 Temperature and precipitation anomalies for austral summer (December–February) during the LIA that were reconstructed using the VCSN/analog circulation pattern selection method. The ensemble mean pattern for both temperature and precipitation was based on the analog years identified from 22 cirque glacier temperature reconstructions. Summer temperature anomalies (*top*) are Celcius while precipitation anomalies (*below*) are mm/season

assumed that unique orographically-driven signatures have not been 'blended' from combining sites that come from more than one climate district. The Oroko Swamp (Cook et al. 2002) summer temperature reconstruction indicates a depression of −0.42 °C relative to the late twentieth century (1961–1990) average. That reconstruction is similar to the summer temperature anomaly that was derived from ELAp of Southern Alps cirque glaciers (Table 1). Negative temperature anomalies are also indicated for the mid-to-late LIA by tree ring reconstructions in north Westland and from Stewart Island (D'Arrigo et al. 1995, 1998). Bacon et al. (2001) have suggested an LIA temperature anomaly of 1 °C below normal based on an ELA depression at Mt. Alarm in the Inland Kaikoura Ranges. While not entirely inconsistent with the findings for individual glacier sites in

this study (Table 1), the LIA glacial geomorphology at Mt. Alarm is not clear, and as such that evidence is disregarded.
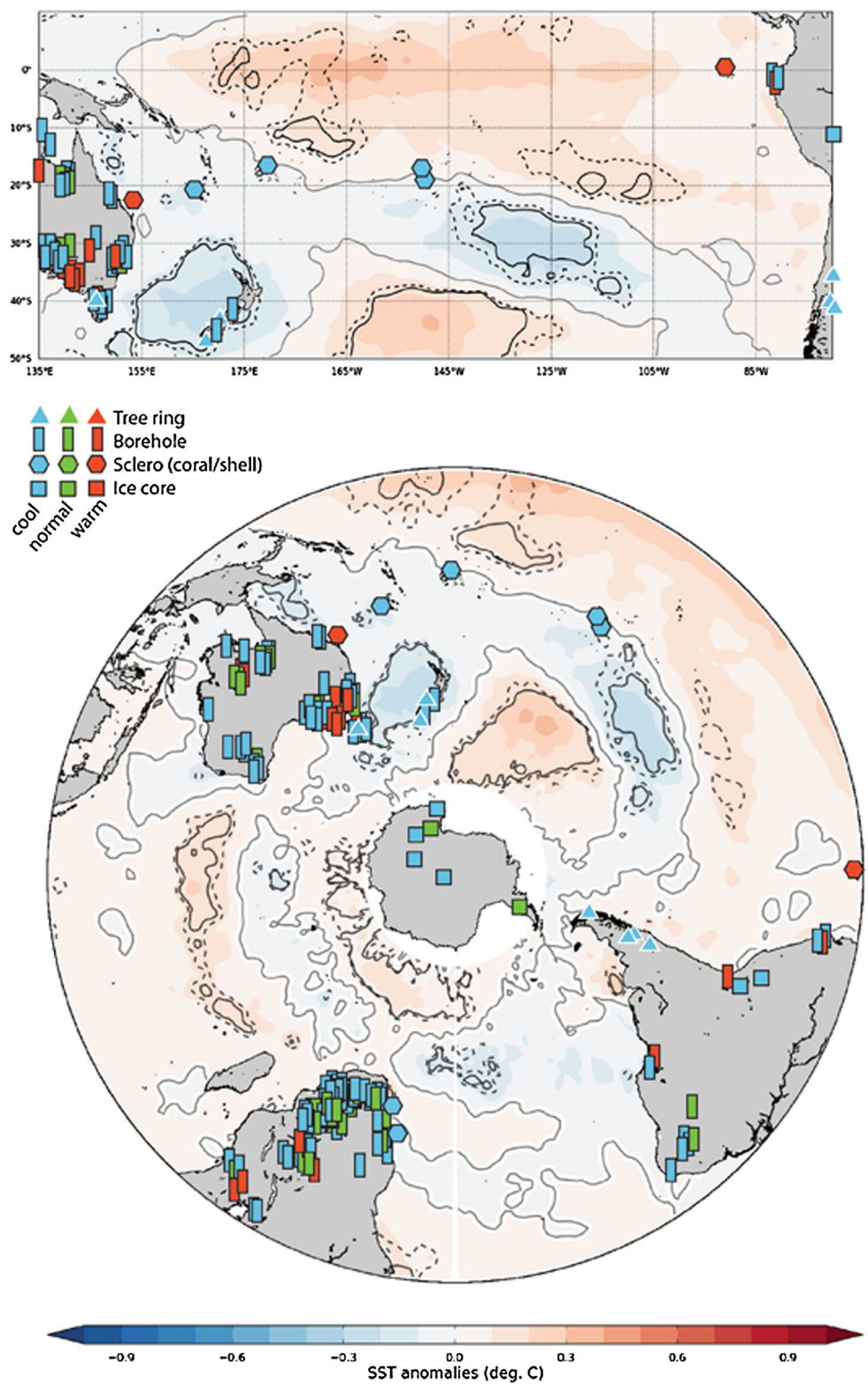
Reconstructed mean annual temperatures (MAT) in the Eastern South Island during the LIA using two borehole sites indicate temperature depressions of −0.9 °C (Whiteford et al. 1996). The difference between the South Island summer temperature reconstructions (Oroko Swamp, Cook et al. 2002; this study) and the mean annual reconstructions (Whiteford et al. 1996) would suggest that winter temperatures were at least 1 °C (and probably close to 1.2 °C) colder on average across much of the South Island during the LIA, if they are taken as regionally-representative. We expect that the inter-regional spatial heterogeneities for LIA temperature and precipitation (north-south and west-east disparities with strong gradients) would also exist or even be amplified at the annual timescale (based on patterns seen in Renwick 2011). Colder winter temperatures relative to summer temperatures during the LIA can reconcile the apparent (minor) incongruence between the reconstructed land-based temperatures from New Zealand derived in this study (Cook et al. 2002) and by others versus apparently colder annual Tasman Sea SSTa (Mann et al. 2009). Relatively more sea ice and general sea ice extension further north in winter relative to summer around Antarctica could have also helped to promote this type of seasonal difference during the LIA, which is supported by palaeoclimate model evidence (Phipps, unpublished; see Supplement). Of importance, the negative SST anomalies seen west of the South Island in our reconstruction reinforce previous work that showed a significant linkage between changes mass balance of Southern Alps glaciers and Tasman Sea temperature (Purdie et al. 2011).

5.1.2 Southwest Pacific

The general central and Southwest Pacific SSTa pattern from our reconstruction is reminiscent of a weak El Niño. Tropical and subtropical Pacific corals show spatial heterogeneity for SSTa (and associated sea surface salinity changes) during the LIA[1] (Fig. 7). Warm anomalies are

---

[1] Sea surface salinity (SSS) and SST changes are two important components that contribute to coral stable oxygen isotope records (Evans et al. 1998; Ren et al. 2002). This can make untangling SST and SSS signals challenging using just δ^{18}O. However, both SST and SSS are commonly modulated by ENSO in the southwest Pacific (Cole et al. 1993; Tudhope et al. 1995; Quinn et al. 1998; Gagan et al. 2000; Linsley et al. 2004, 2006; Asami et al. 2005; Bagnato et al. 2005), which means past marine climate variability is often reported for Pacific coral δ^{18}O records. While ENSO may be an important climate driver for the southwest Pacific and can be recorded in many sclerochronology-based archives (like corals, shells etc.), it is more important for this study that site-specific information about mean climate state rather than past climate driver information or past climate variability is compiled for comparative purposes. Therefore, we focus solely on the records within this proxy type that have provided an SSTa for the LIA.

Fig. 7 Temperature-sensitive proxy signals for the Southwest Pacific region (*top*) and the Southern Hemisphere are superposed on the reconstructed sea surface temperature anomaly field for the LIA. The ensemble mean SSTa patterns were derived using an identical approach as that of z1000 (described earlier in this paper) using analog seasons that were identified by the ELA-based reconstruction of summer temperature for 22 Southern Alps cirque glacier sites. The details for the temperature signals are found in Sect. 5 and Table 2. Cold signatures for boreholes were taken as <−0.25 °C from modern while warm signatures were taken as >+0.25 °C from modern. The 90th and 95th percent (*dashed* and *solid black lines*) confidence intervals are superposed on the plot

reconstructed off the coast of Australia during the late LIA (Hendy et al. 2003) and the Galapagos (Dunbar et al. 1994), while cool SST anomalies are reported for New Caledonia (DeLong et al. 2012), Fiji and the Southern Cook Islands (Goodwin and Harvey 2008; Linsley et al. 2008). The distribution of the southwest Pacific proxy signals compares well with the ensemble composite SSTa pattern that was derived in our glacier-based analysis.

Table 2 LIA palaeoclimate details from selected proxies drawn from sites across the Southern Hemisphere (visually shown in Fig. 7)

Location	Site	Proxy type	Temperature anomaly (°C or qualitative)	Resolution	References
New Zealand	Oroko Swamp	Tree rings	−0.42	Summer	Cook et al. (2002)
New Zealand	North Westland	Tree rings	Cool	Summer	D'Arrigo et al. (1998)
New Zealand	Stewart Island	Tree rings	Cool	Summer	D'Arrigo et al. (1998)
New Zealand	Mt. Alarm	Glacial	−1.00	Summer	Bacon et al. (2001)
New Zealand	Kaikoura	Borehole	−0.90	Annual	Whiteford et al. (1996)
New Zealand	MacRae's Flat	Borehole	−0.90	Annual	Whiteford et al. (1996)
Australia	Central Great Barrier Reef	Coral	Warm	Half-decade	Hendy et al. (2003)
Equatorial Pacific	Galapagos	Coral	Warm	Annual	Dunbar et al. (1994)
Southwest Pacific	New Caledonia	Coral	Cool	Monthly (smoothed 7-months)	Delong et al. (2012)
Southwest Pacific	Fiji	Coral	Cool	Bi-annual	Linsley et al. (2008)
Southwest Pacific	Southern Cook Islands	Coral	Cool	Mean climate state	Goodwin and Harvey (2008)
Australia	Mt. Read, Tasmania	Tree rings	−0.37	Warm season	Cook et al. 2000, 2006
South America	Chile	Tree rings	−0.5 to −1.0	Warm season	Lara and Villalba (1993), Villalba et al. (2003)
South America	Argentina	Tree rings	−0.5 to −1.1	Warm season	Villalba et al. (1997)
South America	Nevado Illimani	Ice core	−0.60	Multidecadal	Kellerhals et al. (2010)
South America	Quelccaya	Ice core	Cool	Half-decade to decadal	Thompson et al. (2006)
South America	Patagonia	Glacial	Cool	Mean climate state	Masiokas et al. (2009a, b)
South America	Multiple sites	Tree rings	Cool	Warm season	Boninsegna et al. (2009)
Antarctica	Vostok	Ice core	Cool		Ekaykin et al. (2004)
Antarctica	Talos Dome	Ice core	Cool	Decadal	Stenni et al. (2002)
Antarctica	Erebus Saddle	Ice core	Cool/normal	Multidecadal	Rhodes et al. (2012)
Antarctica	Dome C, EPICA	Ice core	Cool	Decadal	Mosley-Thompson et al. (1994)
Antarctica	South Pole	Ice core	Variable/cool	Decadal	Mosley-Thompson et al. (1994)
Antarctica	Taylor Dome	Ice core	Variable/cool	Decadal	Steig et al. (2000)
Antarctica	Dyer Plateau	Ice core	Cool		Thompson et al. (1994)
Antarctica	Antarctic Peninsula	Ice core	Warm		Peel et al. (1996)
Antarctica	West Antarctica	Borehole	Cool	Mean climate state	Orsi et al. (2012)
Indian Ocean/South Africa	Ifaty, SW Madagascar	Sclero	Cool	Winter	Zinke et al. (2004)
South Africa	Nelson Bay Cave	Sclero	Cool	Mean climate state	Cohen and Tyson (1995)
South Africa	Makapansgat Valley	Speleothem	Cool	Centennial	Lee-Thorp et al. (2001)

Table 2 continued

Location	Site	Proxy type	Temperature anomaly (°C or qualitative) / Heterogeneous (at continental and hemispheric scales)	Circulation/climate phenomenon anomaly	Resolution / Mean climate state	References
Southern Hemisphere	Multiple sites	Borehole	Heterogeneous (at continental and hemispheric scales)		Mean climate state	Huang et al. (2000)
Antarctica	Erebus Saddle	Ice core		Windy/stronger katabatic winds	Multidecadal	Rhodes et al. (2012)
South Atlantic/South Africa	Offshore of Holgat River	Marine sediment		Stronger coastal upwelling/Agulhas leakage	Multidecadal-centennial	Weldeab et al. (2012)
South America	Multiple sites	Tree ring		Near or above normal MSLP	Warm season	Villalba et al. (1997)
New Zealand	Multiple sites	Tree ring		Near or below normal MSLP	Warm season	Villalba et al. (1997)
Southern Hemisphere	Multiple sites	Tree ring		Negative SAM (equatorward shift of circumpolar jet)	Summer	Villalba et al. (2012)
Antarctica	Law Dome	Ice core		Stronger East Antarctic High/	Multidecadal	Mayewski et al. (2005)
New Zealand	Northern North Island	Tree ring		Reduced ENSO activity and/or weaker ENSO teleconnection pattern	Annual (ENSO cycle-aligned)	Fowler et al. (2012)
Antarctica	Dolleman Island	Ice core		Increased El Nino frequency and negative SAM	Decadal	Russell et al. (2006)
South Africa	Multiple sites	Multiproxy		Equatorward shift/expansion of southern westerlies	Annual to centennial	Tyson and Lindesay (1992)
Antarctica/Indian Ocean	Princess Elizabeth Land	Ice core		Deeper south Indian Ocean low	Decadal	Xiao et al. (2004)
Equatorial Pacific	Washington Island	Lake sediment		Southward displacement of ITCZ/ El Nino-like	Multidecadal-centennial	Sachs et al. (2009)

There is a general indication of near-equatorial warm anomalies, flanked by cool anomalies that extended in a diagonal zone from Papua New Guinea southeast toward the South American coastline.

5.1.3 Tasmania, South America and Antarctica

Reconstructions from tree rings (Tasmania and South America) along with MAT reconstructions from ice cores (Antarctica and South America) and borehole palaeothermometry (global) provide a wider context for mid-to-high latitude temperatures during the LIA. The Huon Pine austral warm season (November–April) temperature reconstruction from Mt. Read, Tasmania indicates LIA was 0.37 °C below the 1961–1990 mean (based on data from (Cook et al. 2000, 2006), while dendroclimatic temperature reconstructions from Chile (Lara and Villalba 1993; Villalba et al. 2003) and Argentina (Villalba et al. 1997) also show colder-than-present average conditions during the LIA (ranging between 0.5 and 1 °C depending on location). Those reconstruction signals are in close proximity to near normal or below normal SSTs that are derived from the glacier-based analysis. In addition, episodic Patagonian Andes glacier advances (Masiokas et al. 2009a, b) provides evidence of a cooler-than-present LIA climate state in southern South America.

Ice core records from Quelccaya suggest negative temperature anomalies between 1450 and 1850 (Thompson et al. 2006), while the ammonium record at Nevado Illimani in the Bolivian Andes indicates temperatures dropped by 0.6 °C between the fifteenth and eighteenth Century (Kellerhals et al. 2010). In Antarctica, Ekaykin et al. (2004) indicate there has been a general temperature increase at Vostok since about 200 years ago, while (Stenni et al. 2002) show a δD record from Talos Dome that is interpreted as a cool interval between 1580 and 1820. (Rhodes et al. 2012) overviewed conditions for the Ross Sea region, and indicated that colder temperatures and stronger winds existed there during the LIA. Comparisons of reconstructions from Talos Dome, Dome C EPICA, South Pole and Taylor Dome (using data of Steig et al. 2000) shows spatial heterogeneity of past temperature across East Antarctica during the LIA (Stenni et al. 2002). Thompson et al. (1994) have also noted near normal conditions at Dyer Plateau in West Antarctica from 1500–1850, while Peel et al. (1996) report warm conditions on the Antarctic Peninsula based on isotope maxima for δ18O and δD during the LIA. Orsi et al. (2012) have indicated cooler WAIS temperatures during the LIA based on a borehole reconstruction, which also suggests spatial heterogeneity of past temperature across West Antarctica during the LIA is plausible.

Borehole reconstructions are numerous (Huang et al. 2000) and show spatially dissimilar land-based LIA

temperature anomalies relative to the time the boreholes were drilled (most during the mid-to-late twentieth Century CE). The indication is that mean climate of Australia was cooler than present during the LIA, with an isolated 'warm' region in southeast Australia. Negative temperature anomalies in the northern part of Australia may have been less severe than in some southern areas, as evidenced by more borehole temperature reconstructions being in the 'normal' range (between ±0.25 °C relative to the modern temperature). The few boreholes that exist for South America show a mix of temperature anomalies in the tropics (both warm and cold) and a warm anomaly close to the two Andean ice core sites. However, the South American tree ring reconstructions (overviewed in Boninsegna et al. 2009) show cool LIA temperatures further south.

5.1.4 Indian Ocean and South Atlantic

The anomalies in the central/south Indian Ocean depict slightly enhanced latitudinal gradients, with the SSTa pattern in that region comparable to a SAM-negative phase. Proxy temperature records surrounding and within South Africa indicate cooler-than-present winter SSTs (Zinke et al. 2004), colder mean SST (Cohen and Tyson 1995; Farmer et al. 2005) and land temperatures (Lee-Thorp et al. 2001), and stronger coastal upwelling with decreased Agulhas leakage into the south Atlantic (Weldeab et al. 2012) during the LIA.

5.2 Southern Hemisphere palaeocirculation patterns of the atmosphere

The southwest Pacific shows weakly negative z1000 anomalies along the Equator to the east of the Dateline. That signature is reminiscent of El Niño-like situations, which typically are accompanied by weaker subsidence (descending air) near Eastern Kiribati, the Marquesas, the Tuamotu Archipelago and French Polynesia during summer. The negative z1000 anomalies are positioned along the northwestern flank of the South Pacific Anticyclone (SPA), a major climatic feature that is linked to both the Hadley and Walker circulation systems (Takahashi and Battisti 2007) that is superposed on the South Pacific Ocean (circumscribed by South Equatorial Counter Current, East Australia Current, Antarctic Circumpolar Current, Humboldt Current). Diminished subsidence in the SPA (at least within the northwestern part of it) would help to weaken easterly Trade Winds along the Equator, reduce blocking in the New Zealand sector, and help the South Pacific Convergence Zone (SPCZ) to shift to the northeast of normal. By association, the corresponding change in the Inter-tropical Convergence Zone (from which the SPCZ branches) would have been in an equatorward direction

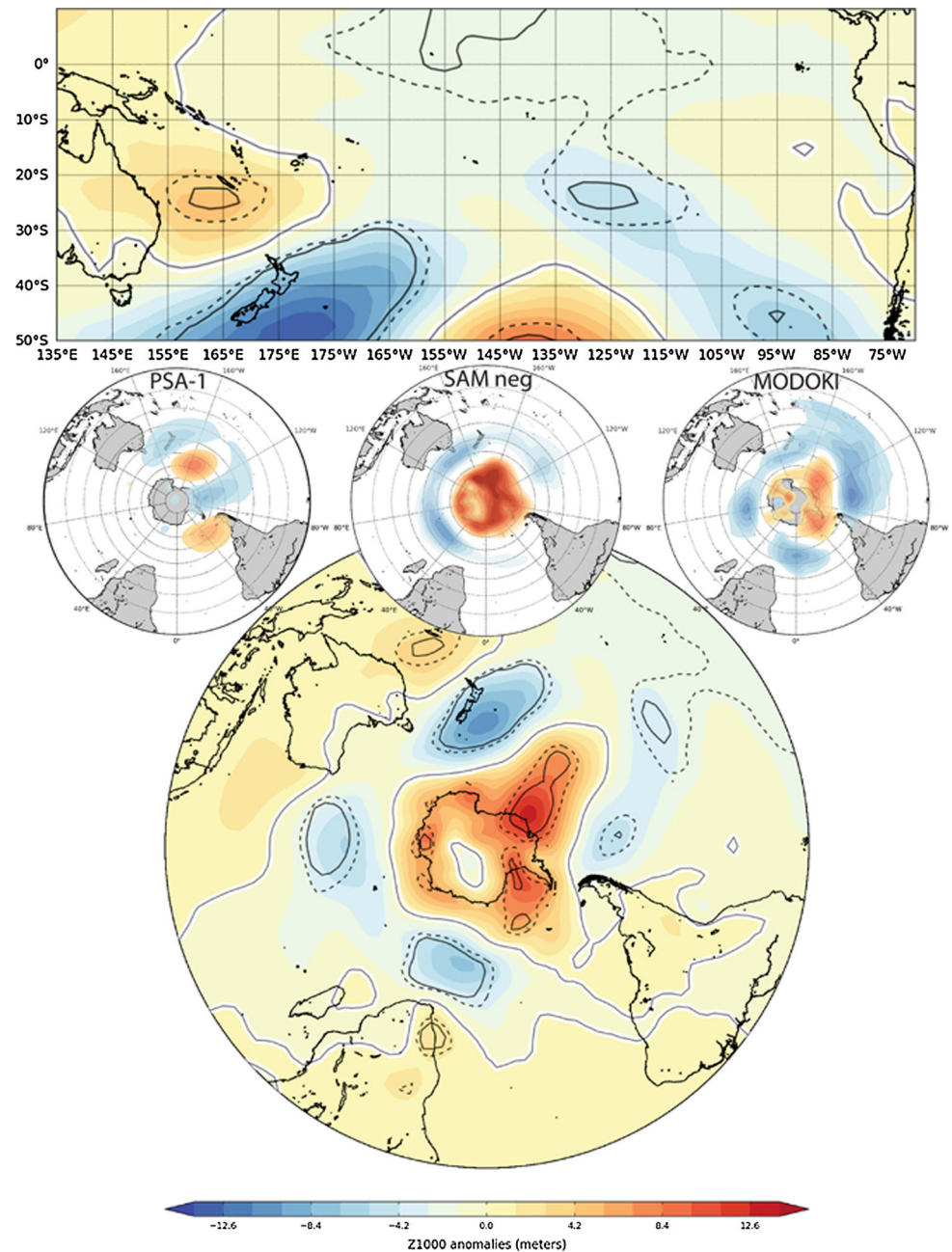during the LIA, which has been suggested by Sachs et al. (2009).

A stronger-than-normal Australian 'high' that is typical of canonical El Niño years is absent in the z1000 reconstruction, although the most prominent anomaly in the subtropics occurs just east of Australia at the boundary of the Coral Sea and Tasman Sea. We also do not observe a typical contiguous positive SST anomaly extending from west of the Dateline eastward to the South American coast in this reconstruction. This lends to the possibility that any potential tropical contribution to the New Zealand LIA atmospheric circulation pattern may have come from a non-typical El Niño variant (i.e., Modoki). Comparisons between z1000 and SSTa for DJF Modoki analogs (following Ashok et al. 2007, 2009) and those from the reconstruction presented in this study show similarities, including near normal geopotential height over most of eastern and northern Australia, relative positions of 'lows', and the relative position of SSTa anomalies in the tropical Pacific (albeit with weaker positive anomaly strength along the Equator in the reconstruction).

Other influences could have contributed to El Niño-like patterns in the tropical Pacific, including the Pacific South American (PSA) mode (Mo and Paegle 2001), which shares a center of action with the atmospheric component of the Southern Oscillation (close to French Polynesia). The PSA has other centers of action over the Southern Ocean to the west of South America and east of the Drake Passage. The SH z1000 pattern is partly consistent with an austral summer PSA-1 pattern, although correspondence is better near New Zealand and east of the Drake Passage, and poorer near the Bellinghausen Sea/Amundsen Sea region through to the eastern edge of the Ross Sea.

Near South Africa, the z1000 anomalies suggest a pressure gradient that would have favored more westerlies during the LIA across the Cape of Good Hope sector. This probably would have served to diminish the leakage into the Atlantic associated with the Agulhas Current, which has also been suggested by preliminary interpretations of new proxy evidence (Weldeab et al. 2012).

The SAM combines with ENSO to produce significant climatic effects in the SH mid latitudes (L'Heureux and Thompson 2006; Ciasto and Thompson 2008; Kidston et al. 2009; Fogt et al. 2011), and influences synoptic type frequencies for New Zealand (Jiang et al. 2012). The most prominent z1000 anomalies in our reconstruction are observed for the SH mid-to-high latitudes and for Antarctica, where a SAM-negative pattern exists. This pattern is characterized by an equatorward shift of the circumpolar trough, with low pressure anomalies positioned between 30 and 60 °S latitude over the south Indian Ocean, the South Atlantic Ocean, New Zealand, and the South Pacific Ocean (akin to a wave pattern 3 and/or 4 configuration). Generally

Fig. 8 Geopotential height anomaly map at 1,000 hPa (z1000) for the Southwest Pacific and the Southern Hemisphere during the LIA. Contour interval for z1000 anomaly is in meters. The 90th and 95th (*dashed* and *solid black lines*) confidence intervals are superposed on the plot. Archetypal patterns of the Pacific South American mode 1 (PSA1), negative Southern Annular Mode (negative SAM) and El Niño Modoki (following analog years identified by Ashok et al. 2007) patterns are shown for reference

positive anomalies over Antarctica are also reminiscent of a SAM-negative signature, with the one exception (albeit, not statistically significant) of a 'low' over the western region of the East Antarctic Ice Sheet.

5.3 Comparison to other atmospheric circulation reconstructions and simulations

Several insights about past atmospheric circulation for the southwest Pacific and the Southern Hemisphere high latitudes during the LIA are relevant for corroborating the findings of this study. Reconstructed MLSP anomalies from Villalba et al. (1997) suggest near-normal or above-normal pressures for the South American sector and near-normal or below-normal MSLP in the New Zealand region during the latter part (1750–1850 CE) of the LIA. That evidence is consistent with the z1000 pattern shown in Fig. 8, and a negative SAM during the LIA (Villalba et al. 2012) that may have been contributed to by solar-induced changes to ozone and westerly circulation (Varma et al. 2012). Mayewski et al. (2005) recognized an atmospheric circulation mode switch in Law Dome ice core geochemistry and attributed it to an increased penetration of El Niño events into high latitudes from 1700–1850 CE to present.

The Law Dome sodium record presented by Mayewski et al. (2005) implies a gradual weakening of the East Antarctic High from the LIA to the present (i.e., it was stronger than present during the LIA), which could have contributed to the sensitivity of high-latitudes to El Niños. The surface pressure anomalies seen in our reconstruction (Fig. 8) are also consistent with that interpretation, and also with the possibility of increased sensitivity of New Zealand to ENSO variability since the LIA (Fowler et al. 2012).

The circulation reconstruction offered by (Russell et al. 2006) from Dolleman Island on the Antarctic Peninsula suggests increased El Niño frequency and lower (more negative) SAM index during the LIA. (Tyson and Lindesay 1992) suggest cooling prevailed from 1350 to 1850 CE (with a warm episode 1500–1675 CE) in South Africa that is consistent with expansion of the circumpolar westerlies. We have not shown the upper level (geostrophic) wind field in this reconstruction, however a more negative SAM, implied from our LIA reconstruction, would be consistent with the South African interpretation of Tyson and Lindesay (1992) and the assessment of Varma et al (2012) for the Chilean sector. Negative z1000 anomalies east of South Africa are consistent with a deeper south Indian Ocean low, which has been proposed from East Antarctic ice core evidence (Xiao et al. 2004). In the Pacific sector, the ITCZ is also proposed to have been located south of climatology (Sachs et al. 2009), which typically coincides with El Niño circulation patterns. El Niños typically produce more frequent westerly-quarter flow across the South Island of New Zealand, which has been proposed as a key control on Southern Alps glacier behavior (Fitzharris et al. 1992, 1997, 2007; Tyson et al. 1997; Lamont et al. 1999; Clare et al. 2002; Purdie et al. 2011). Both the oceanic and atmospheric anomalies in the southwest Pacific region that were reconstructed from this study are consistent with evidence of an El Niño-like climate state during the LIA.

Overall, the suggestion for the LIA atmospheric circulation presented in this study is that multiple Southern Hemisphere climate drivers were conjointly operating in distinct modes to generate an increased (reduced) frequency of trough (blocking) synoptic types over New Zealand. The spatial traits of the atmospheric and sea surface temperature anomalies, when compared to archetypical patterns, suggest two important components may have been El Niño Modoki and the negative phase of SAM. Extracted indices of the SOI, Niño3.4 and SAM from the time 1450–1850 CE timeslice (not shown) suggest the SAM was probably the strongest component helping to dictate atmospheric circulation during the LIA.

We also suggest major climate changes during summer that occurred since the end of the LIA in New Zealand may have resulted from a shift toward positive SAM activity. This shift would have resulted in a decrease in the frequency of trough synoptic types in the New Zealand sector coupled with an increase of blocking synoptic types. It is possible that this change could have been reinforced by stronger ENSO teleconnections to the New Zealand sector (proposed by Fowler et al. 2012) and/or emergence of increased ENSO activity in general through the twentieth century.

6 Conclusions

Southern Alps cirque glacier palaeo-equilibrium lines have provided LIA temperature reconstructions for 22 alpine sites across the South Island of New Zealand. Collectively, these reconstructions suggest a median austral summer temperature depression of $\sim 0.56\ °C$ ($\pm 0.29\ °C$) for the LIA. We have indicated that this regional temperature anomaly was significantly contributed to by daily synoptic type frequencies that were different from present day. Summer atmospheric circulation during the LIA that contributed to the Southern Alps glacier advances was typified by more frequent trough types ('lows') and reduced blocking types ('highs') in the New Zealand sector, and accompanied by colder-than-normal SSTs in the Tasman Sea. Both colder- and wetter-than-normal anomalies are suggested for the mean summer climate state in most regions as a result of this circulation pattern.

Climate changes since the end of the LIA in New Zealand have resulted in Southern Alps glaciers retreating significantly, with less than 1/3rd of the total ice volume remaining from what has been estimated at 1850 CE (Hoelzle et al. 2007; Chinn et al. 2012). Generally, Southern Alps ice recession is associated with negative glacier mass balance, which can be influenced by summer circulation patterns that produce warm conditions over much of the South Island of New Zealand. The findings from this study indicate that an increase in 'blocking' circulation regimes during summer since the LIA lead to an increase in summer temperatures across the Southern Alps that drove ablation. This finding is consistent with previous work linking mass balance changes to regional circulation (Fitzharris et al. 1992; 1997; Tyson et al. 1997; Lamont et al. 1999; Clare et al. 2000; Fitzharris et al. 2007; Purdie et al. 2011). It is also consistent with long-term historic temperature change in New Zealand (Mullan et al. 2010). Our understanding of glacier changes has been improved through this study, however, with the implication of two key synoptic types (the 'T' trough type and 'HSE' blocking type) that were paramount to the LIA climate state and subsequently to twentieth century climate change.

The approach presented in this work (VCSN/analog circulation pattern method) employs similar principles as Regional Climate Regime Classification (RCRC; Lorrey

et al. [2007](#), [2008](#), [2012](#)). The method presented in this study is viewed as a stepwise improvement on RCRC because quantitative pressure anomaly patterns and synoptic type frequency changes have now been produced from multiple terrestrial palaeoclimate reconstructions based in New Zealand. Of importance, the use of a quintile-based analog selection approach for 'calibrating' proxy data means lower resolution and qualitative reconstructions can be used in a similar fashion in forthcoming studies.

The low-frequency centennial-scale spatial pattern for 1450-1850 CE that was observed from the glacier based reconstruction, with support from a collection of supporting proxy archives, has a spatial pattern that is similar to what is observed for the joint operation of two key modern climate drivers (ENSO & SAM) on shorter time scales. Conceptually, Lorrey et al. ([2007](#), [2008](#)) has argued that the self-similar nature of climate variability, in spatial terms, and the low frequency manifestation of palaeoclimate signals through time can be similar to what is observed on high-frequency time scales. The suggestion from this hypothesis is that climate regimes are dictated by synoptic type frequency changes (for New Zealand) that arise from the interplay of multiple climate drivers.

The LIA atmospheric circulation reconstruction and associated SST anomalies along with proxy data across the southwest Pacific and Southern Hemisphere suggest a base climate state during the LIA that was characterized by: (1) weak El Niño -like SST anomalies reminiscent of Modoki in the tropical Pacific, (2) high latitude SST and z1000 anomalies akin to SAM-negative situation (particularly in the south Atlantic and south African sectors), and (3) distinct spatial heterogeneity for Southern Hemisphere surface temperatures. The z1000 circulation pattern suggests, at the very least, that SAM-negative (operating in a planetary wave 3 and/or 4 configuration) and El Niño Modoki conditions probably conspired to contribute to the LIA anomalies for New Zealand. Modern teleconnections to SAM are unchanging from year to year, in broad terms, while ENSO teleconnections vary significantly on interannual to multi-decadal scales. The implications are that the stronger influence of SAM locally in New Zealand may have been enhanced due to a weaker teleconnection with ENSO during the LIA, and/or SAM-dominance was assisted by a mean tropical climate state similar to Modoki. This hypothesis needs further testing with additional proxies from the core region of ENSO activity.

Multiple climate drivers contribute to Southern Hemisphere blocking, amongst which SAM-positive conditions assist the westerly jet in contracting to a more poleward position. This contraction positively reinforces increased anticyclone presence (and a southward dislocation in the subtropical ridge particularly in La Niña years) over New Zealand. It remains the subject of further study to determine the dynamical mechanisms of why a major Southern Hemisphere atmospheric circulation change occurred on entry and coming out of the Little Ice Age. The findings of this study suggest the causes of Southern Hemisphere blocking variability and change over centennial to millennial scales should be a priority for future palaeoclimate work.

References

Ackland JBA (1892) Early explorations at the headwaters of the Rangitata River. N Z Alp J 1:22–30

Anderson B, Mackintosh A (2006) Temperature change is the major driver of late-glacial and Holocene glacier fluctuations in New Zealand. Geology 34:121. doi:10.1130/G22151.1

Asami R, Yamada T, Iryu Y, Quinn TM, Meyer CP, Paulay G (2005) Interannual and decadal variability of the western Pacific sea surface condition for the years 1787–2000: reconstruction based on stable isotope record from a Guam coral. J Geophys Res 110:C05018. doi:10.1029/2004JC002555

Ashok K, Behera SK, Rao SA, Weng H, Yamagata T (2007) El Niño Modoki and its possible teleconnection. J Geophys Res 112:1–27. doi:10.1029/2006JC003798

Ashok K, Iizuka S, Rao SA, Saji NH, Lee W-J (2009) Processes and boreal summer impacts of the 2004 El Niño Modoki: an AGCM study. Geophys Res Lett 36:L04703. doi:10.1029/2008GL036313

Bacon SN, Chinn TJ, Van Dissen RJ et al (2001) Paleo-equilibrium line altitude estimates from late Quaternary glacial features in the Inland Kaikoura Range, South Island, New Zealand. NZ J Geol Geophys 44:55–67

Bagnato S, Linsley BK, Howe SS, Wellington GM, Salinger J (2005) Coral oxygen isotope records of interdecadal climate variations in the South Pacific Convergence Zone region. Geochem Geophys Geosyst 6:Q06001. doi:10.1029/2004GC000879

Boninsegna JA, Argollo J, Aravena JC et al (2009) Dendroclimatological reconstructions in South America: a review. Palaeogeogr Palaeoclimatol Palaeoecol. Elsevier B.V. 281:210–228. doi:10.1016/j.palaeo.2009.07.020

Bradley RS, Briffa K, Cole JE, Hughes MK, Osborne TJ (2003) The climate of the last millennium. In: Pedersen TF, Alverson K, Bradley RF (eds) Paleoclimate, global change and the future. pp 105–141

Cassou C (2008) Intraseasonal interaction between the Madden-Julian Oscillation and the North Atlantic Oscillation. Nature 455:523–527. doi:10.1038/nature07286

Chinn TJ (1996) New Zealand glacier responses to climate change of the past century. NZ J Geol Geophys 39:415–428

Chinn T, Fitzharris BB, Willsman A, Salinger MJ (2012) Annual ice volume changes 1976–2008 for the New Zealand Southern Alps. Global Planet Change 92–93:105–118

Ciasto LM, Thompson DWJ (2008) Observations of large-scale ocean-atmosphere interaction in the Southern Hemisphere. J Clim 21:1244–1259

Clare GR, Fitzharris BB, Chinn TJH, Salinger MJ (2002) Interannual variation in end-of-summer snowlines of the Southern Alps of New Zealand, and relationships with Southern Hemisphere atmospheric circulation and sea surface temperature patterns. Int J Climatol 22:107–120. doi:10.1002/joc.722

Cohen AL, Tyson PD (1995) Sea–surface temperature fluctuations during the Holocene off the south coast of Africa: implications for terrestrial climate and rainfall. The Holocene 5:304–312. doi:10.1177/095968369500500305

Cole JE, Fairbanks RG, Shen GT (1993) Recent variability in the southern oscillation: isotopic results from a Tarawa Atoll Coral. Science 260:1790–1793

Cook ER, Buckley BM, D'Arrigo RD, Peterson MJ (2000) Warm-season temperatures since 1600 BC reconstructed from Tasmanian tree rings and their relationship to large-scale sea surface temperature anomalies. Clim Dyn 16:79–91. doi:10.1007/s003820050006

Cook ER, Palmer JG, D'Arrigo RD (2002) Evidence for a "Medieval Warm Period" in a 1, 100 year tree-ring reconstruction of past austral summer temperatures in New Zealand. Geophys Res Lett 29:1–4

Cook ER, Buckley BM, Palmer JG et al (2006) Millennia-long tree-ring records from Tasmania and New Zealand: a basis for modelling climate variability and forcing, past, present and future. J Quat Sci 21:689–699. doi:10.1002/jqs

D'Arrigo RD, Buckley BM, Cook ER, Wagner WS, Arrigo RDD (1995) Temperature-sensitive tree-ring width chronologies of pink pine (Halocarpus biformis) from Stewart Island, New Zealand. Palaeogeogr Palaeoclimatol Palaeoecol 19:293–300

D'Arrigo RD, Cook ER, Salinger MJ et al (1998) Tree-ring records from New Zealand: long-term context for recent warming trend. Clim Dyn 14:191–199. doi:10.1007/s003820050217

DeLong KL, Quinn TM, Taylor FW, Lin K, Shen C-C (2012) Sea surface temperature variability in the southwest tropical Pacific since AD 1649. Nat Clim Change. Nature Publishing Group 2:799–804. doi:10.1038/nclimate1583

Dunbar R, Wellington GM, Colgan M, Glynn PW (1994) Eastern Pacific sea surface temperature since 1600 A. D'. The record of climate variability in Gahipagos corals we interpret. Paleoceanography 9:291–315

Ekaykin A, Lipenkov V, Kuzmina I, Petit J, Masson-Delmotte V, Johnsen S (2004) The changes in isotope composition and accumulation of snow at Vostok station, East Antarctica, over the past 200 years. Ann Glaciol 39:569–575

Evans MN, Fairbanks RG, Rubenstone JL (1998) A proxy index of ENSO teleconnections. Nature 394:732–733

Farmer EC, DeMenocal PB, Marchitto TM (2005) Holocene and deglacial ocean temperature variability in the Benguela upwelling region: implications for low-latitude atmospheric circulation. Paleoceanography 20:1–16. doi:10.1029/2004PA001049

Fitzharris BB, Hay JE, Jones PD (1992) The Holocene behaviour of New Zealand glaciers and atmospheric circulation changes over the past 130 years. Holocene 2:97–106. doi:10.1177/095968369200200201

Fitzharris BB, Chinn TJ, Lamont GN (1997) Glacier balance fluctuations and atmospheric circulation patterns over the Southern Alps, New Zealand. Int J Climatol 17:745–763

Fitzharris BB, Clare GR, Renwick J (2007) Teleconnections between Andean and New Zealand glaciers. Global Planet Change 59:159–174. doi:10.1016/j.gloplacha.2006.11.022

Fogt RL, Bromwich DH, Hines KM (2011) Understanding the SAM influence on the South Pacific ENSO teleconnection. Clim Dyn 36:1555–1576. doi:10.1007/s00382-010-0905-0

Folland CK, Salinger MJ (1995) Surface temperature trends and variations in New Zealand and the surrounding ocean, 1871–1993. Int J Climatol 15:1195–1218

Fowler AM, Boswijk G, Lorrey AM et al. (2012) Multi-centennial tree-ring record of ENSO-related activity in New Zealand. Nat Clim Change. Nature Publishing Group 2:1–5. doi:10.1038/nclimate1374

Gagan MK, Ayli LK, Beck JW et al (2000) New views of tropical paleoclimates from corals. Quatern Sci Rev 19:45–64

Gellatly AF (1982) Holocene glacial activity in Mt Cook National Park, New Zealand: the use of multi-parameter dating techniques to define glacial moraine chronologies. PhD Thesis, Department of Botany, University of Canterbury

Goodwin ID, Harvey N (2008) Subtropical sea-level history from coral microatolls in the Southern Cook Islands, since 300 AD. Mar Geol 253:14–25. doi:10.1016/j.margeo.2008.04.012

Hendy EJ, Lough JM, Gagan MK (2003) Historical mortality in massive Porites from the central Great Barrier Reef, Australia: evidence for past environmental stress? Coral Reefs 22:207–215. doi:10.1007/s00338-003-0304-7

Hoelzle M, Chinn T, Stumm D, Paul F, Zemp M, Haeberli W (2007) The application of glacier inventory data for estimating past climate change effects on mountain glaciers: a comparison between the European Alps and the Southern Alps of New Zealand. Global Planet Change 56:69–82. doi:10.1016/j.gloplacha.2006.07.001

Huang S, Pollack H, Shen P (2000) Temperature trends over the past five centuries reconstructed from borehole temperatures. Nature 403:756–758. doi:10.1038/35001556

Jiang N, Griffiths G, Lorrey A (2012) Influence of large-scale climate modes on daily synoptic weather types over New Zealand. Int J Climatol doi:10.1002/joc.3443

Kellerhals T, Brütsch S, Sigl M, Knüsel S, Gäggeler HW, Schwikowski M (2010) Ammonium concentration in ice cores: a new proxy for regional temperature reconstruction? J Geophys Res 115:D16123. doi:10.1029/2009JD012603

Kidson JW (2000) An analysis of New Zelaand synoptic types and their use in defining weather regimes. Int J Climatol 20:299–316

Kidston J, Renwick JA, McGregor J (2009) Hemispheric-scale seasonality of the southern annular mode and impacts on the climate of New Zealand. J Clim 22:4759–4770. doi:10.1175/2009JCLI2640.1

Kistler R, Collins W, Saha S et al (2001) The NCEP–NCAR 50–year reanalysis: monthly means CD–ROM and documentation. Bull Am Meteorol Soc 82(2):247–268

L'Heureux ML, Thompson DWJ (2006) Observed relationships between the El Niño–Southern Oscillation and the extratropical zonal-mean circulation. J Clim 19:276–287

Lamont GN, Chinn TJ, Fitzharris BB (1999) Slopes of glacier ELAs in the Southern Alps of New Zealand in relation to atmospheric circulation patterns. Global Planet Change 22:209–219. doi:10.1016/S0921-8181(99)00038-7

Lara A, Villalba R (1993) A 3620-year temperature record from Fitzroya cupressoides tree rings in southern South America. Science 260:1104–1106

Lee-Thorp JA, Holmgren K, Linge H et al (2001) Rapid climate shifts in the southern African interior throughout the mid to late Holocene. Geophys Res Lett 28:4507–4510

Linsley BKK, Wellington GM, Schrag DP, Ren L, Salinger MJ, Tudhope AW (2004) Geochemical evidence from corals for changes in the amplitude and spatial pattern of South Pacific interdecadal climate variability over the last 300 years. Clim Dyn 22:1–11. doi:10.1007/s00382-003-0364-y

Linsley BK, Kaplan A, Gouriou Y et al (2006) Tracking the extent of the South Pacific Convergence Zone since the early 1600 s. Geochem Geophys Geosyst 7:Q05003. doi:10.1029/2005GC001115

Linsley BK, Zhang P, Kaplan A, Howe SS, Wellington GM (2008) Interdecadal-decadal climate variability from multicoral oxygen isotope records in the South Pacific Convergence Zone region since 1650 A.D. Paleoceanography 23:PA2219. doi:10.1029/2007PA001539

Lorrey A, Fowler AM, Salinger J (2007) Regional climate regime classification as a qualitative tool for interpreting multi-proxy palaeoclimate data spatial patterns: a New Zealand case study. Palaeogeogr Palaeoclimatol Palaeoecol 253:407–433. doi:10.1016/j.palaeo.2007.06.011

Lorrey A, Williams P, Salinger J et al (2008) Speleothem stable isotope records interpreted within a multi-proxy framework and implications for New Zealand palaeoclimate reconstruction. Quatern Int 187:52–75. doi:10.1016/j.quaint.2007.09.039

Lorrey AM, Vandergoes M, Almond P et al. (2012) Palaeocirculation across New Zealand during the last glacial maximum at ∼ 21 ka. Quaternary Sci Rev. Elsevier Ltd 36:189–213. doi:10.1016/j.quascirev.2011.09.025

Mann ME (2002) Little Ice Age. Encyclopedia of global environmental change volume 1, the earth system: physical and chemical dimensions of global environmental change. Wiley, New York, 504–509

Mann ME, Zhang Z, Rutherford S et al (2009) Global signatures and dynamical origins of the Little Ice Age and Medieval Climate Anomaly. Science (New York, N.Y.) 326:1256–60. doi:10.1126/science.1177303

Masiokas MH, Luckman BH, Villalba R, Delgado S, Skvarca P, Ripalta A (2009a) Little Ice Age fluctuations of small glaciers in the Monte Fitz Roy and Lago del Desierto areas, south Patagonian Andes, Argentina. Palaeogeogr Palaeoclimatol Palaeoecol. Elsevier B.V. 281:351–362. doi:10.1016/j.palaeo.2007.10.031

Masiokas MH, Rivera A, Espizua LE, Villalba R, Delgado S, Aravena JC (2009b) Glacier fluctuations in extratropical South America during the past 1000 years. Palaeogeogr Palaeoclimatol Palaeoecol. Elsevier B.V. 281:42–268. doi:10.1016/j.palaeo.2009.08.006

Mayewski PA, Maasch KA, White JWC et al (2005) A 700 year record of Southern Hemisphere extratropical climate variability. Ann Glaciol 39:127–132

Mckinzey KM, Lawson W, Kelly D (2004) A revised Little Ice Age chronology of the Franz Josef Glacier, Westland, New Zealand. J R Soc N Z 34:37–41

Meierding TC (1982) Late Pleistocene glacial equilibrium-line altitudes in the Colorado front range: a comparison of methods. Quatern Res 18:289–310

Mo K, Paegle J (2001) The Pacific-South American Modes and their downstream effects. Int J Climatol 21:1211–1229

Mullan A, Stuart SJ, Hadfield MG, Smith MJ (2010) Report on the review of NIWA's "Seven-Station" Temperature series., p 175

Neukom R, Gergis J (2011) Southern Hemisphere high-resolution palaeoclimate records of the last 2000 years. The Holocene 22:501–524. doi:10.1177/0959683611427335

Orsi AJ, Cornuelle BD, Severinghaus JP (2012) Little Ice Age cold interval in West Antarctica: evidence from borehole temperature at the West Antarctic Ice Sheet (WAIS) Divide. Geophys Res Lett 39:L09710. doi:10.1029/2012GL051260

Peel DA, Mulvaney RM, Pasteur EC, Chenery C (1996) Climate changes in the Atlantic sector of Antarctica over the past 500 years from ice-core and other evidence. In: Jones PD, Bradley RS, Jouzel J (ed) Climatic variations and forcing mechanisms of the last 2000 years. Springer, New York, pp 243–262

Purdie H, Mackintosh A, Lawson W, Anderson B, Morgenstern U, Chinn T, Mayewski P (2011) Interannual variability in net accumulation on Tasman Glacier and its relationship with climate. Global Planet Change 77:142–152

Putnam AE, Schaefer JM, Denton GH et al (2012) Regional climate control of glaciers in New Zealand and Europe during the pre-industrial Holocene. Nat Geosci. Nature Publishing Group 5:627–630. doi:10.1038/ngeo1548

Quinn TM, Crowley TJ, Taylor FW, Henin C, Joannot P, Join Y (1998) A multicentury stable isotope record from a New Caledonia coral: interannual and decadal sea surface temperature variability in the southwest Pacific since 1657 A.D. Paleoceanography 13:412–426

Rayner NA, Parker D, Horton E et al (2003) Global analyses of sea surface temperature, sea ice, and night marine air temperature since the late nineteenth century. J Geophys Res 108. doi:10.1029/2002JD002670

Ren L, Linsley BK, Wellington GM, Schrag DP, Hoegh-Guldberg O (2002) Deconvolving the d18 O seawater component from subseasonal coral d 18 O and Sr / Ca at Rarotonga in the southwestern subtropical Pacific for the period 1726 to 1997. Geochim Cosmochim Acta 67:1609–1621

Renwick JA (2011) Kidson's synoptic weather types and surface climate variability over New Zealand. Weather Clim 31:3–23

Rhodes RH, Bertler NAN, Baker JA et al (2012) Little Ice Age climate and oceanic conditions of the Ross Sea, Antarctica from a coastal ice core record. Clim Past 8:1223–1238. doi:10.5194/cp-8-1223-2012

Riddle EE, Stoner MB, Johnson NC, L'Heureux ML, Collins DC, Feldstein SB (2013) The impact of the MJO on clusters of wintertime circulation anomalies over the North American region. Clim Dyn 40(7–8):1749–1766. doi:10.1007/s00382-012-1493-y

Russell A, McGregor GR, Marshall GJ (2006) 340 years of atmospheric circulation characteristics reconstructed from an eastern Antarctic Peninsula ice core. Geophys Res Lett 33(8). doi:10.1029/2006GL025899

Sachs JP, Sachse D, Smittenberg RH, Zhang Z, Battisti DS, Golubic S (2009) Southward movement of the Pacific intertropical convergence zone AD 1400–1850. Nat Geosci. Nature Publishing Group 2:519–525. doi:10.1038/ngeo554

Schaefer JM, Denton GH, Kaplan M et al (2009) High-frequency Holocene glacier fluctuations in New Zealand differ from the northern signature. Science (New York, N.Y.) 324:622–625. doi:10.1126/science.1169312

Sealy EP (1892) Glacier exploration. N Z Alp J 1:54–61

Stenni B, Proposito M, Gragnani R et al (2002) Eight centuries of volcanic signal and climate change at Talos Dome (East Antarctica). 107. doi:10.1029/2000JD000317

Steig EJ, Morse DL, Waddington ED, Stuiver M, Grootes PM, Mayewski PA, Whitlow SI, Twickler MS (2000) Wisconsinan and holocene climate history from an ice core at Taylor Dome, western Ross Embayment, Antarctica. Geografiska Annaler 82A:213–235

Tait A, Henderson R, Turner R, Zheng X (2006) Thin-plate smoothing spline interpolation of daily rainfall for New Zealand using a climatological rainfall surface. Int J Climatol 26:2097–2115

Tait A, Sturman J, Clark M (2012) An assessment of the accuracy of interpolated daily rainfall for New Zealand. J Hydrol (NZ) 51:25–44

Takahashi K, Battisti DS (2007) Processes controlling the Mean Tropical Pacific Precipitation Pattern. Part II: the SPCZ and the Southeast Pacific Dry Zone. J Clim 20:5696–5706. doi:10.1175/2007JCLI1656.1

Thompson L, Peel D, Mosley-Thompson E et al (1994) Climate since AD 1510 on Dyer Plateau, Antarctic Peninsula: evidence for recent climate change. Ann Glaciol 20:420–426

Thompson LG, Mosley-Thompson E, Brecher H et al (2006) Abrupt tropical climate change: past and present. Proc Natl Acad Sci USA 103:10536–10543. doi:10.1073/pnas.0603900103

Tudhope AW, Shimmield GB, Chilcott CP, Jebb M, Fallick AE, Dalgleish AN (1995) Recent changes in climate in the far western equatorial Pacific and their relationship to the Southern Oscillation; oxygen isotope records from massive corals, Papua New Guinea. Earth Planet Sci Lett 136:575–590. doi:10.1016/0012-821X(95)00156-7

Tyson PD, Lindesay JA (1992) The climate of the last 2000 years in southern Africa. The Holocene 2:271–278. doi:10.1177/095968369200200310

Tyson PD, Sturman AP, Fitzharris BB, Mason SJ, Owens IF (1997) Circulation changes and teleconnections between glacial advances on the west coast of New Zealand and extended spells of drought years in South Africa. Int J Climatol 17:1499–1512. doi:10.1002/(SICI)1097-0088(19971130)17:14<1499:AID-JOC207>3.0.CO;2-O

Varma V, Prange M, Spangehl T, Lamy F, Cubasch U, Schulz M (2012) Impact of solar-induced stratospheric ozone decline on Southern Hemisphere westerlies during the Late Maunder Minimum. Geophys Res Lett 39:1–6. doi:10.1029/2012GL053403

Villalba R, Cook ER, D'Arrigo R et al (1997) Sea-level pressure variability around Antarctica since A. D. 1750 inferred from subantarctic tree-ring records. Clim Dyn 13:375–390

Villalba R, Lara A, Boninsegna JA et al (2003) Large-scale temperature changes across the southern Andes: 20th-century variations in the context of the past 400 years. Clim Change 59:177–232

Villalba R, Lara A, Masiokas MH et al (2012) Unusual Southern Hemisphere tree growth patterns induced by changes in the Southern Annular Mode. Nat Geosci doi:10.1038/ngeo1613

Von Haast J (1879) Geology of the provinces of Canterbury and Westland. Times Offices, Christchurch, p 486

Weldeab S, Stuut J-BW, Schneider RR, Siebel W (2012) Holocene climate variability in the winter rainfall zone of South Africa. Clim Past Discuss 8:2281–2320. doi:10.5194/cpd-8-2281-2012

Whiteford P, Allis R, Funnel R (1996) Past surface temperatures from borehole temperature measurements. In: Salinger J (ed) Climate trends in Oceania. Auckland

Winkler S (2000) The "Little Ice Age" maximum in the Southern Alps, New Zealand: preliminary results at Mueller Glacier. The Holocene 10:643–647. doi:10.1191/095968300666087656

Xiao C, Mayewski PA, Qin D, Li Z, Zhang M, Yan Y (2004) Sea level pressure variability over the southern Indian Ocean inferred from a glaciochemical record in Princess Elizabeth Land, east Antarctica. J Geophys Res 109:D16101. doi:10.1029/2003JD004065

Zinke J, Dullo W-C, Heiss GA, Eisenhauer A (2004) ENSO and Indian Ocean subtropical dipole variability is recorded in a coral record off southwest Madagascar for the period 1659 to 1995. Earth Planet Sci Lett 228:177–194. doi:10.1016/j.epsl.2004.09.028